State of the Art in Time-Dependent Flow Topology: Interpreting Physical Meaningfulness Through Mathematical Properties

Roxana Bujack[†1] , Lin Yan[‡2] , Ingrid Hotz[§3] , Christoph Garth[¶4] , Bei Wang[‖2]

[1]Los Alamos National Laboratory, USA
[2]Scientific Computing and Imaging Institute, University of Utah, USA
[3]Scientific Visualization Group, Linköpings University, Sweden
[4]University of Kaiserslautern, Germany

Abstract

We present a state-of-the-art report on time-dependent flow topology. We survey representative papers in visualization and provide a taxonomy of existing approaches that generalize flow topology from time-independent to time-dependent settings. The approaches are classified based upon four categories: tracking of steady topology, reference frame adaption, pathline classification or clustering, and generalization of critical points. Our unique contributions include introducing a set of desirable mathematical properties to interpret physical meaningfulness for time-dependent flow visualization, inferring mathematical properties associated with selective research papers, and utilizing such properties for classification. The five most important properties identified in the existing literature include coincidence with the steady case, induction of a partition within the domain, Lagrangian invariance, objectivity, and Galilean invariance.

1. Introduction

Motivation. Vector field topology has seen widespread applications since its introduction to visualization by Helman and Hesselink [HH89] more than 30 years ago. For steady flows, it is one of the most promising tools to extract relevant information from the data. It is utilized from two important perspectives, first to compress the data in a structure-preserving way with little information loss, and second to reduce occlusion in visualization.

A considerable amount of research has focused on the topology of time-independent (steady) vector fields via the notion of the *topological skeleton*, which consists of *critical points* and specific streamlines called *separatrices* that partition the domain into areas of uniform flow behavior. While vector field topology works well for electric and magnetic vector fields, it looses physical meaning for time-dependent (unsteady) flows. In particular, it is difficult to interpret flow topology in the time-dependent setting.

On the other hand, an instantaneous snapshot of a vector field and the streamlines arising from it do not describe time-dependent behavior. This is a problem that is not exclusive to flow topology. For example, Lugt [Lug79] encounters a similar problem while trying to define a vortex.

---

† bujack@lanl.gov
‡ lin.yan@utah.edu
§ ingrid.hotz@liu.se
¶ garth@cs.uni-kl.de
‖ beiwang@sci.utah.edu

> An instantaneous streamline picture does not give enough information to identify a vortex and, thus, cannot be used to define a vortex.
>
> *Lugt [Lug79]*

Similarly, Perry and Chong [PC94a] describe that it is difficult to interpret vector field topology in unsteady flows.

> In the study of the topology of flow patterns and eddying motions, instantaneous streamlines have found considerable use even though they are not Galilean invariant and appear to lose physical meaning if the flow is unsteady.
>
> *Perry and Chong [PC94a]*

Due to the limited applicability of vector field topology, the study of time-dependent flow topology remains heterogeneous and fragmentary. This topic is also embedded in the larger context of dynamical systems, in particular for the purpose of visualization. Even though some mature techniques and systematic methodologies have been developed for the study of time-dependent flow topology, we hope to impose mathematical structures on existing techniques to ease their access for researchers and practitioners.

Contributions. In this paper, we survey and organize the scattered literature on time-dependent flow topology, discuss recent results, and identify research gaps.

It is our intention to assist both beginners and experts in navigating the field of flow visualization in a time-dependent setting. In particular, our work is motivated by the following two questions essential to time-dependent flow topology:

- How can time-independent vector field topology be generalized to the time-dependent setting in a *physically meaningful* way?
- How can the notion of *physical meaningfulness* for flow visualization be characterized rigorously?

To addressing these questions, our contributions are:

- We provide a survey and a classification of approaches used to generalize vector field topology from the time-independent to the time-dependent settings, based on four categories: tracking of steady topology, reference frame adaption, pathline classification or clustering, and generalization of critical points.
- We collect desirable mathematical properties to interpret the notion of *physical meaningfulness* for time-dependent flow visualization, namely: coincidence with the steady topology, induction of a partition, Lagrangian invariance, objectivity, and Galilean invariance.
- We analyze and infer mathematical properties associated with selected approaches, making it easy to identify current challenges and opportunities.

Overall, we provide an organized classification of the literature for time-dependent flow topology. As a majority of works address the 2D case, we give it proportionally more attention.

Admittedly, there is not a single, general, and universally agreed upon definition for the notion of "physically meaningfulness". By talking to physicists, we have learned that the meaning of this notion changes from problem to problem in the sense that "if a method answers my question, then it is physically meaningful." We will try to narrow down what this notion means by collecting mathematical concepts that are used in the literature in the sense that "this method is not physically meaningful because it does not satisfy a particular set of mathematical properties." However, it is important to note that the properties we collect are not exhaustive, and they do not *define* but rather *interpret* physical meaningfulness.

Our contributions are summarized in Tables 1- 4. Each table contains the related works that belong to one of the four categories of approaches. The columns correspond to the five desirable properties. Each table cell is color-coded to indicate whether a method satisfies a particular property and contains a reference for a more detailed example or theorem.

Related surveys. Topology-based techniques have received substantial attention from survey authors in recent years. The surveys by Laramee *et al.* [LHZP07] and Wang *et al.* [WWL16] both contain discussions on unsteady flows in terms of topology extraction. Furthermore, Pobitzer *et al.* [PPF*11a] and Heine *et al.* [HLH*16a] provide classifications of time-dependent vector field topology. Laramee *et al.* [LCJK*09] also give an overview of the application of flow topology in science and engineering.

Our approach differs fundamentally from these earlier efforts. In addition to classifying available techniques, we organize relevant works by the problems they try to address, and collect mathematical properties that encompass the notion of *physical meaningfulness*. In many practical scenarios, the notion of physical meaningfulness is problem-specific and application-driven; here, we collect and apply mathematically rigorous definitions that are desirable with respect to such a notion. Our core contribution and the most important

difference with respect to earlier surveys is that we embed all relevant approaches from the literature into a mathematical framework encoding desirable properties of physical meaningfulness. For a surveyed technique, if a description regarding a particular property of interest is not readily available, we infer such a property on the basis of mathematical reasoning. Subsequently, we are able to clearly identify gaps, challenges, and opportunities in current research, which complement existing state-of-the-art reports in vector field visualization.

We explicitly exclude discussions on Lagrangian coherent structures and feature detection in flow fields (such as vortices), since these topics belong to large fields of study that have been surveyed recently, see [HFB*17, PVH*03, GT18].

Outline. This paper is organized as follows. Sec. 2 describes our survey procedure and classification guidelines. Sec. 3 briefly reviews the technical foundations of flow topology. Sec. 4 details the classification of current approaches involving time-dependent flow topology; and Sec. 5 describes flow characteristics relevant to time-dependent data and proves their associated mathematical properties. Sec. 6 reviews relevant papers in time-dependent flow topology beyond visualization, such as fluid dynamics and dynamic systems. Sec. 7 gives a discussion on emerging research directions. Sec. 8 concludes the paper.

2. Literature Research Procedure and Classification

We review representative papers in the field of visualization that contain methods that generalize (or can be extended to generalize) vector field topology from the time-independent to the time-dependent settings. The annotation of each paper is guided primarily by a set of four *categories* that classify common approaches (related to existing surveys [PPF*11a, HLH*16a]), see Sec. 2.1.1 to Sec. 2.1.4; and secondarily by a set of five desirable *properties* that are mathematically definable (untreated in previous works), which encompass Sec. 2.2.1 to Sec. 2.2.5.

2.1. Classification Based on the Approach

Our comprehensive literature review allows us to identify four major categories of time-dependent flow topology approaches, according to which we classify the literature. Some papers fit into more than one category as they are hybrid methods or suggest several approaches. They will be listed multiple times here, but they will be treated in detail only once in Sec. 4.

We define an "approach" as the main principle upon which a method is based. The four categories we choose have been proven useful in existing literature, and research papers that fall into each category perform similar analysis tasks or share similar mathematical foundations.

2.1.1. Tracking of Steady Topology

The straightforward approach to extend flow topology to unsteady case applies the classical (steady) vector field topology to each time step [HH89, HH90, WSH01, TSH01, TWSH02, TS03, TWHS04, TWHS05, WTVGP11, RKWH12, GTS04, SW14]. We collect methods in this category if they perform feature tracking in

the time-dependent setting where features are coming from time-independent vector field topology, see Sec. 4.1.

2.1.2. Reference Frame Adaption

As pointed out in the quote by Perry and Chong [PC94a] (Sec. 1), a (chosen) frame of reference is key in flow analysis. Even though reference frame adaption is not specifically designed for flow topology, it is a promising approach for a physically meaningful generalization [WGS02, BPB14, BPKB14, FKS*10, BHJ16, WBPRH17, HMTR18, GGT17, RG20].

We call an approach frame of reference (FOR) adaptive if specific global or local FORs are chosen with the goal of making streamlines meaningful in a time-dependent setting, see Sec. 4.2.

2.1.3. Pathline Classification or Clustering

Pathlines are considered to have a clear physical meaning in the sense that they describe the movement of massless particles and coincide with streamlines for steady fields. Therefore the classification of pathlines is a very promising approach to generalize flow topology [TWHS04, TWHS05, SW10, USE12, WCW*11, MBES16, HKTH16, WRT18, BDBR*19, BDZG19].

An approach is considered to classify or cluster pathlines if it chooses distinguished pathlines, labels them, or groups them together based on their properties. The difference between pathline classification and pathline clustering is that classification is supervised learning where predefined labels are assigned to instances based on their characteristics, whereas clustering is unsupervised learning where similar instances are grouped together based on similarity measures or metrics, see Sec. 4.3.

2.1.4. Generalization of Critical Points

Another popular approach uses derived characteristics of the flow, usually Galilean invariant scalar fields, and makes use of structurally or topologically significant points, like zeros or extrema, in these scalar fields [SW10, USE12, KHNH11, RKWH12, KRH*16, FKS*10, BHJ16, MBES16, WBPRH17].

We say an approach generalizes the definition of a critical point from the time-independent setting if it uses flow characteristics other than the zeros of the velocity. Techniques in this category can make use of the scalar field topology to derive segmentations and simplifications, frame of reference adaptions for visualizations that are related to the classical ones, or Lagrangian smoothing to highlight Lagrangian behavior, see Sec. 4.4.

2.2. Classification Based on Desirable Properties

We survey existing research works not only for how they generalize flow topology from time-independent to time-dependent fields, but also for which mathematical properties these works possess or imply. Certain methods enjoy a subset of the following five mathematical properties, which have been identified as important to establish physical meaningfulness. We chose these properties because they are the most popular ones suggested in the existing literature. These properties have been motivated in scattered places, whereas our paper systematically specifies and investigates these properties and their relations to relevant mathematical concepts.

2.2.1. Coincidence With the Steady Flow Topology

> Taking one step back, the overall goal is to find methods that can give comparable answers for unsteady flow as vector field topology (VFT) for steady flow...
>
> *Pobitzer et al. [PPF*11b]*

Our literature search did not come across many explicit statements of the desirable property for a method to coincide with the steady vector field topology, except a few [PPF*11a, KHNH11, FKS*10, RG20]. Perhaps this is a basic requirement that previous authors did not feel the need to explicitly state.

Assuming the input to a method is a steady flow field, i.e., it does not change over time, then the features extracted by this method are identical to the critical points and separatrices of the steady setting. Mathematically speaking, let $v : \mathbb{R}^d \to \mathbb{R}^d$ be a steady flow field and let $F(\cdot)$ be an operator that extracts time-independent topology. Suppose we have an unsteady flow field $v_t : \mathbb{R}^d \times \mathbb{R} \to \mathbb{R}^d$ that is defined over space and time, but not changing over time, that is, there exists a steady field $v : \mathbb{R}^d \to \mathbb{R}^d$ such that $\forall t \in \mathbb{R} : v_t(x,t) = v(x)$. Let $F_t(\cdot)$ be an operator that extracts time-dependent topology. Then for a method designed to extract features of an unsteady field, we would like its output to coincide with the steady flow topology when it is applied to v_t, that is, $F_t(v_t(x,t)) = F(v(x))$ for $(x,t) \in \mathbb{R}^d \times \mathbb{R}$.

2.2.2. Induction of a Partition of the Domain

> ...namely to segment the flow domain into parts with coherent properties in terms of their temporal evolution.
>
> *Pobitzer et al. [PPF*11b]*

One of the most important properties of the steady vector field topology is that it implies a partition of the domain into areas of coherent flow behavior. Such an induced partition is also a desirable property for its generalizations in the unsteady setting [PPF*11b, HLH*16a, RG20].

We say that a method *induces a partition of the domain* in the time-dependent setting if it has a concept of generalized separatrices that segment the domain of space and time into subsets $S_i \subset \mathbb{R}^d \times \mathbb{R}$. The set $\{S_i\}$ forms a partition if $\forall i \neq j : S_i \cap S_j = \emptyset$ and $\bigcup_i S_i = \mathbb{R}^d \times \mathbb{R}$. We explicitly require that the partition is not generally trivial for finite times, i.e., $S_i \neq \mathbb{R}^d \times \mathbb{R}$. The difference is illustrated in Fig. 6.

2.2.3. Lagrangian Invariance

> Therefore, we can require the boundaries of a time-dependent topological skeleton to be material surfaces and the unsteady critical points to be fluid particles.
>
> *Fuchs et al. [FKS*10]*

Pathlines describe the paths of fluid particles. It is a popular criterion for physical meaningfulness to demand the extracted features to be Lagrangian invariant [SLM05, FKS*10, Hal15, HKTH16, HFB*17, BDBR*19, BDZG19].

A method is *Lagrangian invariant* if the features it extracts move over time as if they were advected by the flow. Explicitly, let $S(t) : \mathbb{R} \to \mathbb{R}^d$ be an extracted feature over time and $F_{t_0}^t(x_0) :$ $\mathbb{R} \times \mathbb{R} \times \mathbb{R}^d \to \mathbb{R}^d$ the flowmap (Sec. 5.1.6) indicating where a massless particle starting at time t_0 at location x_0 moves to until time t. Then, $S(t)$ is Lagrangian invariant if $\forall t : F_{t_0}^t(S(t_0)) \subseteq S(t)$. For line features, this is equivalent to the extracted line to be tangential to the flow $\forall t \in \mathbb{R} : \dot{S}(t) \times v(S(t), t) = 0$.

2.2.4. Objectivity

> Frame-invariance is particularly important in truly unsteady flows, which have no distinguished frame of reference.
>
> *Hadjighasem et al. [HFB*17]*

One of the most popular properties used in the literature to indicate that a concept is physically meaningful is objectivity [TN04, Hal05, RSM16, HFB*17, GGT17, HMTR18, RG20, BDBR*19, BDZG19].

A method is *objective* if the extracted features do not change under a Euclidean change of the reference frame. Precisely, let $\chi_{S(t)}(x,t) : \mathbb{R}^d \times \mathbb{R} \to \{0,1\}$ be the characteristic function indicating if a point in spacetime belongs to an extracted feature over time $(x,t) \in S(t)$. Furthermore, let $x' = Q(t)x + r(t) \in \mathbb{R}^d$ be a change of coordinates with a time-dependent orthogonal matrix $Q : \mathbb{R} \to SO(d)$ and a time-dependent vector $r : \mathbb{R} \to \mathbb{R}^d$. Then, the feature is objective if $\chi'_{S(t)}(x',t) = \chi_{S(t)}(x,t)$, see Sec. 5.1.

2.2.5. Galilean Invariance

> It is only when Galilean frame of reference can be found which gives an almost steady velocity field that we have a velocity pattern with some useful physical meaning.
>
> *Perry and Chong [PC94a]*

Galilean invariance is a special case of objectivity, where the extracted features do not change under a Galilean change of the reference frame. It is often used as a minimal requirement to ensure that something has physical meaning [PC94b, SH95, SWTH07, Wie08, KHNH11, FKS*10, PPF*11b, SW10, USE12, MBES16, BHJ16, WBPRH17].

A concept is *Galilean invariant* if two observers in moving reference frames with relatively constant velocity relative to each other observe a phenomenon in the same way. Mathematically, this is a special case of objectivity where the rotation is a constant $Q \in SO(d)$ and the translation is linear $\dot{r} = const \in \mathbb{R}^d$ in the transformation $x' = Qx + r(t)$, see Sec. 5.1.

3. Technical Foundations on Vector Field Topology

Vector fields are used to model physical phenomena of interest across many scientific fields. The field of fluid dynamics, in particular, gives rise to large and complex flow fields. Initiated by Helman and Hesselink [HH89], vector field topology has developed into an integral part of the analysis and visualization of flow fields. However, since vector field topology considers only the behavior of streamlines, it is especially appropriate to capture structures in steady flow fields. In this section, we briefly review main ingredients of steady vector field topology. After introducing topological features for 2D and 3D vector fields, we give a generalized perspective from dynamic systems.

3.1. 2D Vector Field Topology

A 2D vector field $v : D \subseteq \mathbb{R}^2 \to \mathbb{R}^2$ assigns a 2D vector to each point in the domain D, where v is assumed to be continuous and differentiable. In the steady setting, v can be expressed as

$$v(x,y) = \begin{pmatrix} v_1(x,y) \\ v_2(x,y) \end{pmatrix}. \tag{1}$$

2D vector field topology consists of critical points, periodic orbits, and separatrices.

A *critical point* $x \in D$ is an isolated zero in the vector field, that is, $v(x) = (0,0)^T = \mathbf{0}$, and $v(y) \neq \mathbf{0}$ for any $y \neq x$ in a small neighborhood of x. Critical points can be classified with respect to their *Poincaré indices*. The Poincaré index of a critical point x counts the positive field rotations while traveling along a simple closed curve containing x in a positive direction. In 2D, critical points such as *sources*, *sinks*, and *centers* have indices $+1$, whereas *saddles* have indices -1.
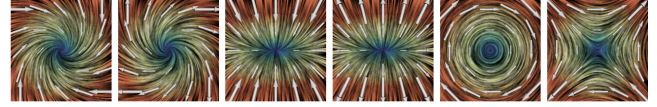

Figure 1: *Categories of classical critical points based on the eigenvalues of the Jacobian. From left to right: spiral sink and source (also known as attracting/repelling foci), node sink and source (also known as attracting/repelling nodes), center, and saddle. Flows are visualized via arrow glyphs and line integral convolution (LIC) [CL93]; color represents speed from low (blue) to high (red) values. Image reproduced from Bujack et al. [BHJ16].*

An alternative classification of critical points is based on the eigenvalues of the *Jacobian matrix* J_v containing the first derivatives of the vector field

$$J_v(x,y) = (\frac{\partial v}{\partial x}, \frac{\partial v}{\partial y},) = \begin{pmatrix} \frac{\partial v_1(x,y)}{\partial x} & \frac{\partial v_1(x,y)}{\partial y} \\ \frac{\partial v_2(x,y)}{\partial x} & \frac{\partial v_2(x,y)}{\partial y} \end{pmatrix} \tag{2}$$

The determinant of J_v is called the *Jacobian* of the vector field. A critical point x is a *first-order* critical point if the Jacobian does not vanish in x; otherwise, it is called a *high-order* critical point. The classification of critical points could be further refined based on eigenvalues of J_v to include attracting nodes/foci and repelling nodes/foci, centers, and saddles, see Fig. 1 and [HH89, Fig. 5].

A *streamline* is a line that is tangential to the instantaneous velocity direction, see Fig. 2. Mathematically, a streamline $s(t)$ is a curve in the domain of v, where for any t,

$$\dot{s}(t) = v(s(t)). \tag{3}$$

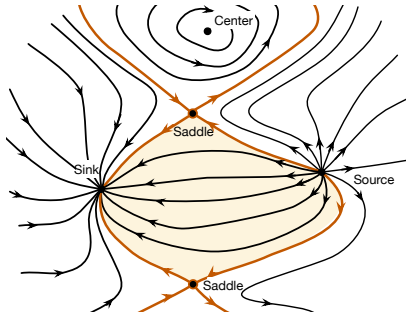Here, t is not the time but refers to an arbitrary parameterization of

Figure 2: *Topology of a simple vector field. The yellow area is a region where all streamlines start in the same source and end in the same sink. The brown streamlines are separatrices.*

the curve. *Closed orbits* are closed streamlines, which means there is a parameter τ such that $s(t) = s(t + \tau), \forall t \in \mathbb{R}$.

Separatrices are the bounding streamlines that separate the regions of uniform streamline behavior. Assuming only first-order critical points, they emerge from the saddle points along the directions of the eigenvectors of the Jacobian. Finally, *vector field topology* consists of critical points and separatrices that segments the domain in regions of uniform streamline behavior, see Fig. 2.

3.2. 3D Vector Field Topology

A 3D vector field $v : D \subseteq \mathbb{R}^3 \to \mathbb{R}^3$ assigns a 3D vector to each point in the domain D, where v is assumed to be continuous and differentiable. 3D vector field topology consists of critical features and separating features. Critical features are critical points, periodic orbits, and complex 2D structures such as strange attractors. The separatrices become separating surfaces emerging from saddle points, compare Fig. 3.
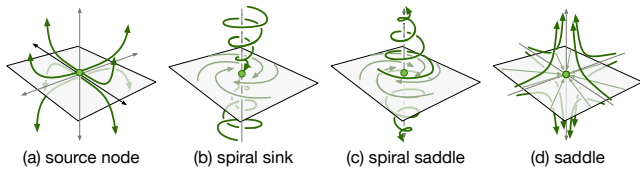

| (a) source node | (b) spiral sink | (c) spiral saddle | (d) saddle |

Figure 3: *Examples of critical points in 3D linear vector fields. In 3D, separating surfaces emerge from saddle points (c,d).*

Critical points are defined similarly to the 2D case as isolated zeros in the vector field, that is, $v(x) = (0,0,0)^T = \mathbf{0}$, and $v(y) \neq \mathbf{0}$ for any $y \neq x$ in a small neighborhood of x. Critical points are commonly classified based on the eigenvalues of the *Jacobian matrix* J_v. A critical point x is a *first-order* critical point if the Jacobian does not vanish in x; otherwise, it is called a *high-order* critical point. First-order critical points include attracting source and sink nodes/spiral, and saddles, see Fig. 3.

3.3. From the Perspectives of Dynamical Systems

The main ingredients of vector field topology have been studied in dynamical systems, namely, *limit sets*, *separating lines*, and *sepa-*

rating surfaces. Let $v : D \subseteq \mathbb{R}^d \to \mathbb{R}^d$ denote a d-dimensional vector field. Let c_p denote a streamline passing through a point $p \in D$. In its most general form, the limit sets of a streamline, referred to as α-limit set and ω-limit set, are defined as

$$
\begin{aligned}
A(c_p) &= \Big\{ q \in D | \exists (t_n)_{n=0}^{\infty} \subset \mathbb{R} \text{ with } \lim_{n \to \infty} t_n = -\infty \\
&\qquad \text{such that } \lim_{n \to \infty} c_p(t_n) = q \Big\} \\
\Omega(c_p) &= \Big\{ q \in D | \exists (t_n)_{n=0}^{\infty} \subset \mathbb{R} \text{ with } \lim_{n \to \infty} t_n = \infty \\
&\qquad \text{such that } \lim_{n \to \infty} c_p(t_n) = q \Big\}
\end{aligned}
\tag{4}
$$

The explicit form of the limit sets varies depending on the dimension of the vector field. These sets are best researched for the 2D case, where the limit sets consist of *critical points*; which are classified according to the streamline behavior in their vicinity (see Sec. 3.1). Streamlines are considered to be equivalent if their limit sets coincide, meaning a streamline has the same origin set (α-limit set) and the same end set (ω-limit set). In 2D, streamlines that are on the boundary of equivalent streamlines are the *separating lines*; in 3D, they become *separating surfaces*; in higher-dimensions, they are *separating manifolds*. The topological skeleton therefore consists of limit sets and separating manifolds in high dimensions.

4. Classification

The core contribution of this paper is the classification of existing works, which are summarized in Tables $1 - 4$. Each table contains the papers that belong primarily to one of the four approaches (see Sec. 2.1). Based on the underlying mathematical concepts of each paper, each row contains our inference of its mathematical properties. For each cell (i, j), green means that the paper in row i satisfies the property in column j, red means that it does not satisfy the property; teal means that it *mostly* satisfies the property; and purple means that it *mostly does not* satisfy the property, see Fig. 4. The text in each cell provides either a short sketch of the mathematical reasoning behind our decision or a reference to a counter example or a theorem in Sec. 5.

| Yes. | Mostly yes. | Mostly no. | No. |

Figure 4: *Legend for Tables $1 - 4$. The colors indicate if a method does or does not satisfy a mathematical property.*

The best way to explore our classification is to use each table as a roadmap, which leads to specific examples and theorems in Sec. 5. In other words, the tables serve as an *overview*, whereas the examples and theorems are *details on demand* [Shn03].

Disclaimer. For each surveyed paper, we use our best judgement to infer mathematical properties associated with its proposed techniques. Our inference is based on the technical formulations from each paper and sometimes its code (if available). However, we do not claim that we have perfectly captured the authors' intentions.

We summarize the properties of different methods in Tables 1–4 by connecting them with the mathematical concepts upon which they are mainly based. We did not implement the algorithms of surveyed papers. The proofs and counterexamples we provide are designed for mathematical concepts, not for specific methods. The

proofs provided in each cell are not always rigorous; they are sometimes sketches of the underlying ideas using simple examples, e.g., a vector field in 1D. It is important to also note that different methods require different properties of the underlying data, such as smoothness or piecewise linearity, which we do not explicitly treat to keep the presentation concise.

4.1. Tracking of Steady Topology

Given the success of vector field topology in the steady case, it is natural to track topological features over time in the unsteady case. The goal is to correctly associate features from one time step to the next, as well as to detect and represent events that change the topology, such as merges, splits, births, and deaths of critical points.
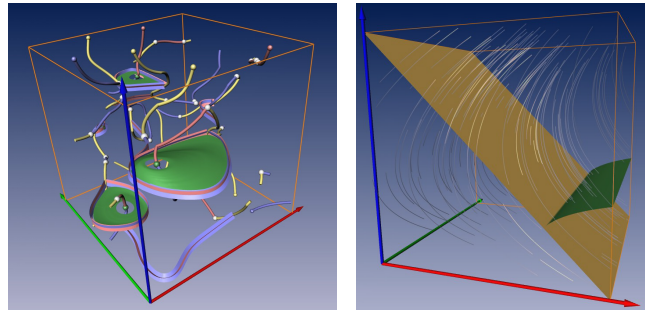
Helman and Hesselink [HH89, HH90] provide a tracking algorithm over time. They compute the singularities (critical points) for separate time steps, and connect them graphically based on proximity and region connectedness. Wischgoll *et al.* [WSH01] describe an algorithm to track closed streamlines in time-dependent planar flows. Based on an earlier algorithm [WS01] that uses the Poincaré-Bendixson theorem, their tracking scheme assumes linear interpolation between two time steps and detects bifurcations. Tricoche *et al.* [TSH01, TWSH02] provide a precise tracking algorithm, assuming a linear interpolation between time steps. The linear interpolation in their spacetime grid guarantees the existence of one critical point in each cell. Therefore, it is sufficient to analyze the cell faces to detect changes in the topology over time. Inside each cell, they employ analytical paths between singularities.

Theisel and Seidel [TS03] derive Feature Flow Fields (FFF) that recast the tracking of critical points in a 2D vector field as an integration problem in a 3D field. They show that their technique can be utilized to track other topological features and vortices. Weinkauf *et al.* [WTVGP11] improve upon the FFF and present a more stable FFF formulations for tracking critical points. Reininghaus *et al.* [RKWH12] propose a combinatorial version of this concept.

Theisel *et al.* [TWHS04, TWHS05] follow two approaches to the generalization of topology to unsteady vector fields. In their streamline-based method, they track the topology of each time step interpreted as steady flow, see Fig. 5.

Garth *et al.* [GTS04] provide a singularity tracking algorithm for 3D time-dependent vector fields. Analogously to [TSH01], they use piecewise linear fields to guarantee that topological changes can occur only on the boundary of cells. They also use the principal axis of all singularity to reduce visual clutter, and a diagram over time to capture the evolution of the underlying topology.

Skraba and Wang [SW14] infer correspondences between critical points based on their closeness in stability, measured by robustness, instead of just distance proximities within the domain. Intuitively, the robustness of a critical point is the minimum amount of perturbation necessary to cancel it. They prove formally that robustness helps us understand the sampling conditions under which we can resolve the correspondence problem based on region overlap techniques, and the uniqueness and uncertainty associated with such techniques. These conditions also provide a theoretical basis for visualizing the piecewise linear realizations of critical point trajectories over time.

(a) *Tracking of the classical streamline-based vector field topology.* **(b)** *Partition generated by the pathline-based topology.*

Figure 5: *Examples of the streamline- and pathline-based vector field topology. Image reproduced from Theisel et al. [TWHS04, TWHS05].*

All the above methods share a similar goal in terms of feature tracking, which induces identical mathematical properties. These mathematical properties are summarized in Table 1. The surveyed methods trivially coincide with the steady case and segment the domain of the flow; however, they are neither Lagrangian nor Galilean invariant, and therefore are not objective. Table 1 highlights the shortcomings of the steady vector field topology, which some authors refer to as being "unphysical".

4.2. Reference Frame Adaption

Most methods that adapt the frame of reference (FOR) are not specifically targeting flow topology, but they provide derived vector fields, which can be visualized or processed. For this survey, we analyze these methods assuming that we apply classical steady vector field topology to the derived fields. Please note that most of the methods in this section do not actually suggest a conservative coordinate transform of the form $x' = Q(t)x + r(t)$. What they all have in common with a classical FOR adaption is that they try to compensate for or subtract out the influence of a potential common underlying movement of regions in the flow.

Wiebel *et al.* [WGS02] suggest a segmentation of the flow field into a potential, a divergence, and a rotation part, using the Helmholtz Hodge decomposition (HHD). The potential part is identical to the flow on the boundary and therefore correlates with the influence of the outer flow onto a region. Its removal reveals local structures in the flow that would otherwise be hidden. Bhatia *et al.* [BPB14, BPKB14] suggest a flow decomposition method that follows the HHD, which decomposes the flow into irrotational, incompressible, and harmonic parts. Whereas Wiebel *et al.* [WGS02] assume the boundary flow to be zero, Bhatia *et al.* do not require boundary conditions to be unique, thereby reducing the complexity of their method for compressible flows. Bhatia *et al.* compute the HHD of a derived field that is identical to the flow inside the region but drops to zero at infinity. Its harmonic component is zero, which makes the HHD unique. They then utilize only the irrotational and incompressible parts restricted to the region in question.

Günther *et al.* [GGT17] provide an algorithm to locally assume

Tracking of steady topology					
paper	coincide with steady case	segment areas of coherent behavior	Lagrangian	Galilean invariant	objective
[HH89, HH90, WSH01, TSH01, TWSH02, TS03, WTVGP11, GTS04, SW14], [TWHS04, TWHS05] (streamline-based), [RKWH12] (using $v = 0$)	each time step is the steady case	separatrices as (hyper-) surfaces in $d + 1$	Example 1	dependence on velocity (8), Example 2	dependence on velocity (8), Example 2

Table 1: Mathematical properties and references to examples for papers primarily classified under **tracking of steady topology**. Color coding is explained in Fig. 4.
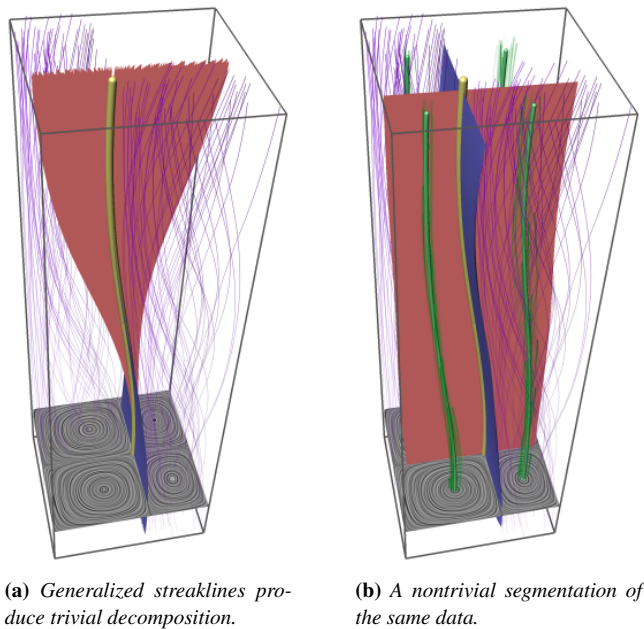

(a) *Generalized streaklines produce trivial decomposition.*

(b) *A nontrivial segmentation of the same data.*

Figure 6: *Generalized streaklines that start at a saddle-type pathline are used (for example, in [SW10, USE12, MBES16, BDBR*19, BDZG19]) to separate regions of different behavior locally. These streamlines produce a trivial segmentation overall if the field is given for only a finite time and a comparable nontrivial decomposition. In this spacetime representation: saddles are yellow, centers are green, generalized separatrices are red, and pathlines are purple. Image reproduced from Rojo et al. [RG20, Fig. 3].*

Figure 7: *Reference frame "steadification". Top: spacetime representation; bottom: space representation. Instantaneous velocity is visualized through LIC [CL93] in grey; pathlines are visualized in color. Image reproduced from Hadwiger et al. [HMTR18].*

the FOR that makes the field appear mostly steady. Such a local FOR is considered the best frame to view flow patterns, for example, by Lugt [Lug79] and Perry and Chong [PC94a]. Günther *et al.* decompose the minimization requirement so that they need to solve only a system of linear equations. Later, Rojo *et al.* [RG20] extract steady topology using similar local FOR, see Fig. 6. They provide a pathline-based visualization for context.

Hadwiger *et al.* [HMTR18] propose a time-dependent velocity field describing the motion of a set of observers adapted to the input flow. The *observer field* is defined such that all observers perceive the flow to be "as st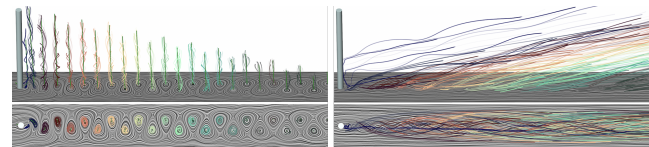eady as possible" with almost vanishing time derivatives. An observer-related time derivative is defined, which builds on the concept of Lie derivatives. The observer field minimizes this observed time derivative using global optimization, see Fig. 7. Based on this observer field, notions of observed streamlines, pathlines, streaklines, and timelines are introduced. Hadwiger *et al.* prove that the flow perceived by the observer field is objective, making the derived flow features, such as vortices, objective as well. Even though a topological segmentation is not explicitly discussed in the paper, the derived field can be used to define an objective flow topology.

The above papers follow two main objectives. Wiebel *et al.* [WGS02] and Bhatia *et al.* [BPB14, BPKB14] make use of the HHD because of its useful properties and applications. They are less focused on the frame invariance and do not show Galilean invariance in their papers. Günther *et al.* [GGT17, RG20] and Hadwiger *et al.* [HMTR18], on the other hand, specifically design reference frame adaptions to meet frame invariance. Whereas the former coincides with the steady case, the latter produces smooth results due to its global nature. We can see in Table 2 how the methods satisfy more desirable properties. An obvious observation is the apparent lack of Lagrangian invariance for methods in the current category of reference frame adaption.

4.3. Categorize or Cluster Pathlines

Pathlines are tangential to a vector field everywhere in time, but streamlines are tangential for one fixed point in time. In a steady vector field, pathlines and streamlines coincide, which motivates researchers to select, categorize, and cluster pathlines to generalize flow topology. Pathlines describe the movement of particles, which gives them direct physical meaning.

Theisel *et al.* [TWHS05] categorize areas of convergent behav-

Reference frame adaption					
paper	coincide with steady case	segment areas of coherent behavior	Lagrangian	Galilean invariant	objective
[WGS02]	Example 3	separatrices as (hyper-) surfaces in $d+1$	Example 6	Theorem 1	Example 4
[BPB14, BPKB14]	Example 3	separatrices as (hyper-) surfaces in $d+1$	Example 6	Theorem 1	Example 5
[HMTR18]	Theorem 2, Example 7	separatrices as (hyper-) surfaces in $d+1$	Example 8	Sec. 4.3 in their paper refers to proof in [TN04]	Sec. 4.3 in their paper refers to proof in [TN04]
[GGT17, RG20]	$v_t = 0$ is already optimum	separatrices as (hyper-) surfaces in $d+1$	Example 9	Sec. 3.1 of the additional material of [RG20], but not for linear fields, Sec. 7.10 in [GGT17]	Sec. 3.2 of the additional material of [RG20], but not for linear fields, Sec. 7.10 in [GGT17]

Table 2: Mathematical properties and references to proofs for papers classified as primarily **reference frame adaption**. Most of the reference frame adaption techniques were derived for general visualization techniques, and the papers do not specifically mention flow topology. For the purpose of this report, we categorize them under the assumption that the classical vector field topology is applied to the frame adapted field. Color coding is explained in Fig. 4.

ior, divergent behavior, or neither using pathlines as extensions of sinks, sources, and saddles, see Fig. 5.
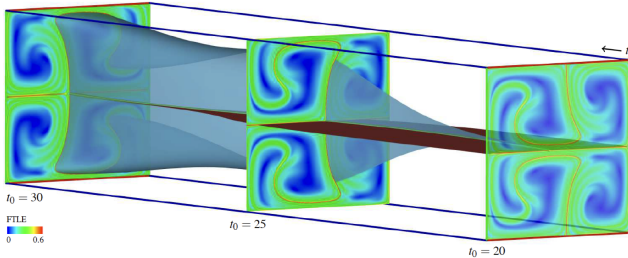

Figure 8: *First generalization of separatrices to generalized streaklines. Spacetime visualization with slices are color-coded by FTLE: attracting manifolds are in blue, repelling manifolds are in red. Image reproduced from Sadlo and Weiskopf et al. [SW10].*

Inspired by Haller's hyperbolic trajectories [Hal00], Sadlo and Weiskopf [SW10] generalize the concept of saddle-type critical points to time-dependent vector fields using the intersections of ridges in the forward and backward *finite-time Lyapunov exponent field (FTLE)* [Hal02a]. FTLE is a scalar measure describing the amount of stretching of neighboring pathlines during a time interval $[t, t+t']$ respective to $[t, t-t']$. The motivation behind this choice is the same as that for saddles: these areas show divergent behavior in forward as well as backward direction in time. They use these points as seeds for generalized streaklines as introduced by Wiebel *et al.* [WTS*07], which form a generalization of separatrices to time-dependent flows, see Fig. 8. They also look into

ridges in the hyperbolicity time fields, but discard the approach as unsatisfactory in practice. The work of Sadlo and Weiskopf is an important step toward a time-dependent flow topology. The counterparts of centers, sources, and sinks are, however, still missing.
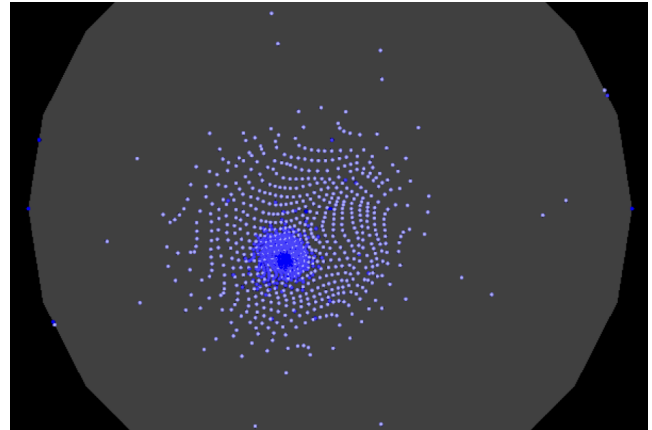

Figure 9: *Particle accumulation over time indicates a sink in the famous Petri-dish dataset. Particles are color-coded by time of seeding. Image reproduced from Wiebel et al. [WCW*11].*

Wiebel *et al.* [WCW*11] start pathlines at a set of timepoints. At any given end time, they compute the density of endpoints of pathlines and track the local maxima of this histogram-like scalar field as the time-varying analog of sinks. Their approach provides a physically meaningful visualization of a very complicated dataset involving a rotating Petri dish, see Fig. 9.

Üffinger *et al.* [USE12] extend earlier work [SW10] to a 3D case by computing streak-based separatrices from 1D seeding curves. The latter are obtained from path surfaces emanating from 2D ridges in forward and reverse FTLE fields.
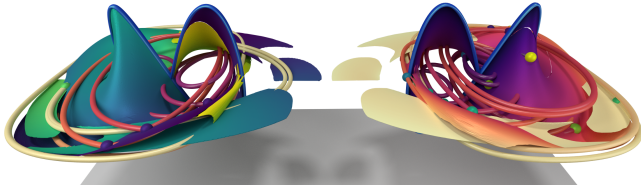

Figure 10: *Example of a recirculation surface. This method produces truly steady visualizations, i.e., features that do not depend on time. Color encodes start time (left) and integration time (right). Image reproduced from Wilde et al. [WRT18, Fig. 1].*

Wilde *et al.* [WRT18] present a method to extract recirculation surfaces for 3D unsteady flow fields. The key idea is to embed the flow in a higher dimensional manifold for the line extraction and then project the results back to the 3D space. A recirculation line is defined as a pathline that returns to the same location after some time. There is no requirement that the flow direction is the same after returning to the point, see Fig. 10. Wilde *et al.*'s paper is an exception in this category of methods as it does not aim to generalize vector field topology. However, we include this paper in the survey, because the idea of a 5D displacement field could hypothetically be used for categorize or cluster pathlines, even though the displacement field is frame dependent.
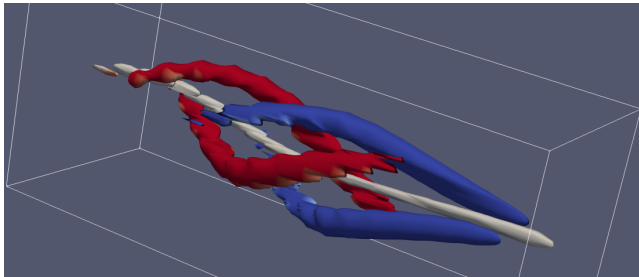

Figure 11: *Spacetime representation of a nontrivial segmentation over time of a rotating field into regions with source-like (red), sink-like (blue), and saddle-like behavior (white). Other regions are transparent. Image reproduced from [BDZG19].*

Bujack *et al.* [BDBR*19] follow the work of Sadlo and Weiskopf [SW10] to extract pathlines of strong hyperbolic behavior as finite-time saddles. In contrast to earlier work, they introduce a Lagrangian definition using the full range of time moments that are captured in the dataset. They further suggest a more robust classification based on forward and backward integration time separately and show that it is a sufficient criterion for its Lagrangian counterpart. Later they extend this definition and categorize pathlines as sinks, sources, or saddles based on their finite time expansion or contraction behavior over the whole simulation time [BDZG19], see Fig. 11. The results are areas that segment the domain and narrow down toward the true critical point locations if a longer integration time is available.

Table 3 shows the mathematical properties of these approaches. We see that even though the first use of pathline-based topology by Theisel *et al.* [TWHS05] is a great idea, the actual implementation does not improve the frame independence or Lagrangian shortcomings of the classical topology. The works followed satisfy frame independence by concentrating on certain types of features, such as only saddles and separatrices [SW10, USE12, BDBR*19], and only sinks [WCW*11], until the theoretical concepts are unified in a framework spanning saddle-, source-, and sink-type regions [BDZG19]. The methods in this category are partly not Lagrangian even though they are pathline-based, because they do not use the whole time available. This choice can be motivated by one of the two following reasons. First, a sliding window approach may produce more intuitive and visually pleasing results, because it does not capture the chaotic folding and mixing. Second, a Lagrangian method may exhibit issues w.r.t. robustness or stability because it requires integration on an unstable manifold for a long time. These methods can be made Lagrangian if they are applied to the full time interval of the data.

4.4. Generalization of Critical Points

This section comprises a direction of research that explicitly follows the goal of generalizing the classical vector field topology to unsteady fields or changing frames of reference. These methods make use of scalar fields and utilize their extrema (or zeros) to define generalized critical points.
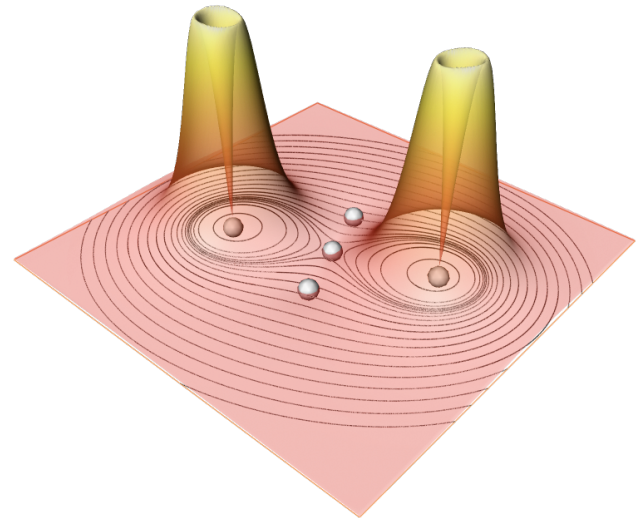

Figure 12: *Acceleration magnitude is shown as a colored height map and the extracted minima (spheres) serve as generalized critical points. Image reproduced from Kasten et al. [KHNH11].*

Kasten *et al.* [KHNH11, KRH*16] extend the concept of critical points to the minima of the acceleration field. This extension includes the classical definition of critical points in steady fields, but is Galilean invariant. They filter these candidates using a version of Lagrangian filtering. They track two scalar properties over parts of a pathline: the acceleration and the minimality. When a

Categorize or cluster pathlines					
paper	coincide with steady case	segment areas of coherent behavior	Lagrangian	Galilean invariant	objective
[TWHS04, TWHS05] (pathline-based)	extracts regions, instead of critical points	each point is assigned one category	Fig. 5b shows pathlines intersect the boundaries	Example 10	Example 10
[SW10, USE12]	saddles only, but Example 11	Fig. 6 (a)	sliding time window, Sec. 2.3 in [Hal15]	eigenvalues of the Cauchy Green tensor, Sec. 5.1.9	eigenvalues of the Cauchy Green tensor, Sec. 5.1.9
[WCW*11]	sinks only, but Example 11	not intended or discussed	sliding time window, Sec. 2.3 in [Hal15]	density proportional to distance between particles, Sec. 5.1.7	density proportional to distance between particles, Sec. 5.1.7
[WRT18]	critical points only	surfaces do not induce partition, self-intersection	method does not produce time-dependent features, but can be extended	distance between particles in different times, Sec. 5.1.10	distance between particles in different times, Sec. 5.1.10
[BDBR*19]	saddles only, but Example 11	Fig. 6 (a)	sufficient condition, Sec. 4.2 in [BDZG19]	eigenvalues of the Cauchy Green tensor, Sec. 5.1.9	eigenvalues of the Cauchy Green tensor, Sec. 5.1.9
[BDZG19]	extracts regions, instead of critical points	Fig. 17, but not for incompressible flow	sufficient condition, Sec. 4.2 in [BDZG19]	eigenvalues of the Cauchy Green tensor, Sec. 5.1.9	eigenvalues of the Cauchy Green tensor, Sec. 5.1.9

Table 3: *Mathematical properties and references to proofs for papers classified as primarily* **categorize or cluster pathlines***. Color coding is explained in Fig. 4.*

pathline violates one of the thresholds, they stop considering it critical. Then, they consider only those pathlines that have a life-time above a given threshold. A major problem is that the time parameter needs to be much smaller for saddle-like critical points than for centers, see Fig. 12. Related to that is the work by Reininghaus *et al.* [RKWH12], who propose a combinatorial tracking algorithm for critical points in scalar fields. They apply the method to track classical critical points of flows as well as the generalized critical points from the acceleration minima by Kasten *et al.* [KRH*16]. In theory, the tracking method itself is independent of the FOR as long as the scalar field used for the definition of the critical points is Galilean invariant. In practice, however, the required temporal sampling density of the flow filed depends on the strength of the background flow. Consequently, the tracking of critical points from steady vector field topology is not Galilean invariant, and the tracking of zeros in the acceleration is invariant if the temporal sampling density is high enough.

Fuchs *et al.* [FKS*10] extend the concepts of the steady-state critical points to time-varying data in four different ways. They first look at the zeros of the acceleration. Then they suggest that each detected point adapts the FOR to become a classical critical point. They classify these points in the classical sense, which allows for locally meaningful separatrices. To compensate for more complex FOR changes, Fuchs *et al.* suggest selecting particles that observe an almost steady velocity in their vicinity and have a small acceleration. To this end, they introduce the concept of unsteadiness as the material derivative of the Jacobian. Further, they apply Lagrangian smoothing to both unsteadiness and the velocity. They

show that Lagrangian filtering applied to the velocity magnitude, acceleration magnitude, and unsteadiness provides results that are comparable to the FTLE in the double gyre. For an analytic version of the Petri dish, on the other hand, only Lagrangian smoothed unsteadiness gives results similar to those of the FTLE.
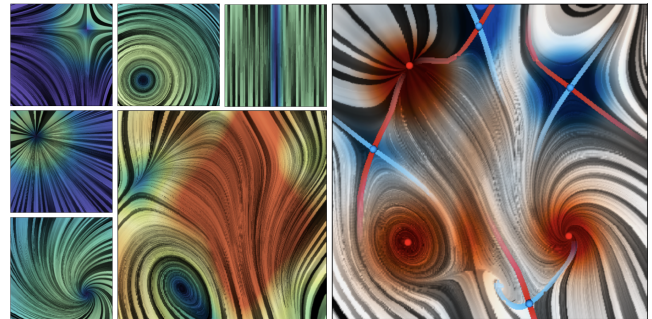

Figure 13: *The local reference frames (right) of the generalized critical points reveal the individual components (left, small) of a supercomposition (left, big) of different fields. The vector field is visualized by LIC [CL93] and colored by speed on the left: blue means low and red means high values. The vector field is colored by determinant of the Jacobian on the right: blue means negative, red means positive, and white means zero values. Image reproduced from Bujack et al. [BHJ16].*

Bujack *et al.* [BHJ16] suggest dropping the requirement of a critical point to have zero velocity because a FOR always exists that

can make it critical. Since the categorization of the critical points into sink, sources, saddles, and centers is Galilean invariant, they suggest critical points be generalized as extrema of the determinant of the Jacobian. Then, they locally assume FOR for these points in the visualization, see Fig. 13.

Wang *et al.* [WRS*13] use the topological concept of robustness, which is related to persistence in the scalar case. This concept reflects how much a vector field needs to be perturbed such that a critical point gets canceled. They track the robustness of critical points over time. However, since the physical meaning of classical critical points is doubtful under reference frame changes, they apply the measure of robustness not only to critical points but also to any point in its own reference [WBPRH17], which makes the method Galilean invariant.

Machado *et al.* [MBES16] extract hyperbolic trajectories as pathlines close to bifurcation lines in the extended phase space, i.e., the spacetime representation of the vector field. They argue that these pathlines and their invariant manifolds produce LCS like the intersection of forward and backward FTLE ridges and like the material surfaces started at these intersections (from [SW10] but faster). For the definition of bifurcation lines, they follow Roth *et al.* [Rot00, RP98] and use the loci where the velocity v is parallel to either the steady formulation of acceleration $a = (\nabla v)v$ or the jerk vector $b = (\nabla a)v$. They refine the results to form streamlines as in their prior work [MSE13]. Because the results were poor, they abandon the jerk vector approach and use the acceleration. For the case of the spacetime field, the condition $x \times a = 0$ is equivalent to loci with vanishing acceleration $a = 0$, which shows the relation to previous techniques [KPH*09, FKS*10].

Table 4 summarizes the techniques from this section and their properties. The table shows that the scalar characteristics were chosen to be Galilean invariant, but not objective. The method by Machado *et al.* [MBES16] stands out, particularly because it constitutes a hybrid approach between these scalar-field-based techniques and the pathline-based methods from Sec. 4.3.

5. Theory

In this section, we provide a detailed mathematical analysis summarized in Tables 1–4. The tables provide an *overview* of our classification results. Each table cell refers to a part in this section, which provides *details on demand* in the form of a proof sketch or a (counter) example. We first revisit the behaviors associated with basic flow characteristics that are frequently used by the surveyed methods under coordinate transformations. Then, we provide examples and theorems to infer the properties of these methods. Again, the surveyed papers are classified by approaches as detailed in Sec. 2.1.

5.1. Coordinate Transformations

In this section, we collect the mathematical concepts and flow characteristics that are used to generalize the classical (i.e., time-independent) vector field topology to time-dependent data and analyze their properties under changes of the reference frame. We then focus on determining for which one of the desirable properties a

suggested method suffices. An introduction to the physical principles can be found, for example, in [Liu02, SJ06].

We look at Euclidean transformations of coordinates $(x,t) \in \mathbb{R}^d \times \mathbb{R}$, i.e., transformations of the form

$$x' = Q(t)x + r(t) \tag{5}$$

with a time-dependent orthogonal matrix $Q : \mathbb{R} \to SO(d)$ and a time dependent vector $r : \mathbb{R} \to \mathbb{R}^d$ [TN04].

A Galilean transformation is a subset of (5) with the additional restriction of r depending only linearly on time, $\dot{r} = const$.

A scalar field $s(x,t)$, a vector field $v(x,t)$, and a matrix field $M(x,t)$ are called *objective*, i.e., invariant with respect to a coordinate transformation, [Son13] if they suffice

$$\begin{aligned} s'(x',t) &= s(x,t), \\ v'(x',t) &= Q(t)v(x), \\ M'(x',t) &= Q(t)M(x,t)Q^T(t). \end{aligned} \tag{6}$$

5.1.1. Velocity Field

The classical steady vector field topology and the tacking of topological features [HH89, HH90, WSH01, TSH01, TWSH02, TS03, WTVGP11, GTS04, SW14, TWHS04, TWHS05, RKWH12] use the definition of critical points as zeros in the velocity field

$$v(x,t) = \frac{dx(t)}{dt} = \dot{x}. \tag{7}$$

The velocity field is not invariant under the transformation (5) as

$$\begin{aligned} v'(x',t) &\stackrel{(7)}{=} \frac{dx'}{dt} \\ &\stackrel{(5)}{=} \frac{d}{dt}(Q(t)x + r(t)) \\ &= \dot{Q}(t)x + Q(t)\dot{x} + \dot{r}(t) \\ &\stackrel{(7)}{=} \dot{Q}(t)x + Q(t)v(x,t) + \dot{r}(t). \end{aligned} \tag{8}$$

Therefore, (8) means that v is neither objective nor Galilean invariant.

5.1.2. Galilean Invariant Vector Field

Some methods [FKS*10, BHJ16, WBPRH17] use the Galilean invariant vector field (GIVF) following a Galilean transform to perceive a given point x_0 as critical

$$v_{x_0}(x,t) = v(x,t) - v(x_0,t). \tag{9}$$

Transformation (5) transforms $v'(x',t)$ via

$$\begin{aligned} v'_{x'_0}(x',t) &\stackrel{(8)}{=} v'(x',t) - v'(x'_0,t) \\ &\stackrel{(8)}{=} \dot{Q}(t)x + Q(t)v(x,t) + \dot{r}(t) \\ &\quad - (\dot{Q}(t)x_0 + Q(t)v(x_0,t) + \dot{r}(t)) \\ &= Q(t)(v(x,t) - v(x_0,t)) + \dot{Q}(t)(x - x_0). \end{aligned} \tag{10}$$

Therefore according to (10), v_{x_0} is not objective but Galilean invariant; v_{x_0} is referred to as the Galilean invariant critical points.

Generalization of critical points					
paper	coincide with steady case	segment areas of coherent behavior	Lagrangian	Galilean invariant	objective
[KHNH11, RKWH12, KRH*16]	sufficient condiction Example 12	not intended or discussed	Example 13	dependence on acceleration, Sec. 5.1.3	dependence on acceleration, Sec. 5.1.3
[FKS*10]	Thm. 3	separatrices are meaningful only locally	Example 13	dependence on acceleration, Sec. 5.1.3, unsteadiness, Sec. 5.1.5, Jacobian, Sec. 5.1.4, GIVF, Sec. 5.1.2	dependence on acceleration, Sec. 5.1.3, unsteadiness, Sec. 5.1.5, Jacobian, Sec. 5.1.4, GIVF, Sec. 5.1.2
[BHJ16]	Example 14	connected components of same determinant sign	Example 14	dependence on Jacobian, Sec. 5.1.4, GIVF, Sec. 5.1.2	dependence on Jacobian, Sec. 5.1.4, GIVF, Sec. 5.1.2
[MBES16]	saddles only Thm. 3	Fig. 6 (a)	Example 15	Example 15	Example 15
[WBPRH17]	Example 16	not discussed but provided through Morse complex of extended robustness field	Example 16	dependence on GIVF, Sec. 5.1.2	dependence on GIVF, Sec. 5.1.2

Table 4: Mathematical properties and references to proofs for papers classified as primarily **generalization of critical points**. Color coding is explained in Fig. 4.

5.1.3. Acceleration

The acceleration field [KHNH11, FKS*10, RKWH12, MBES16, KRH*16] is the material derivative of the flow field

$$a(x,t) = \ddot{x}$$
$$\overset{(7)}{=} \frac{Dv(x,t)}{Dt}$$
$$= \frac{dv(x,t)}{dx}\frac{dx}{dt} + \frac{\partial v(x,t)}{\partial t} \qquad (11)$$
$$\overset{(7),(13)}{=} J(x,t)v(x,t) + \frac{\partial v(x,t)}{\partial t}.$$

On the other hand, a transforms via (11), (5) and (7),

$$a'(x',t) = \frac{d^2 x'(t)}{dt^2}$$
$$\overset{(11)}{=} \frac{d^2}{dt^2}(Q(t)x + r(t))$$
$$\overset{(5)}{=} \ddot{Q}(t)x + 2\dot{Q}(t)\dot{x} + Q(t)\ddot{x} + \ddot{r}(t), \qquad (12)$$
$$\overset{(7),(11)}{=} \ddot{Q}(t)x + 2\dot{Q}(t)v(x,t) + Q(t)a(x,t) + \ddot{r}(t),$$

which makes it Galilean invariant, but not objective.

5.1.4. Jacobian

The Jacobian of a velocity field is the velocity gradient

$$J(x,t) = \nabla_x v(x,t). \qquad (13)$$

The Jacobian is typically used to classify classical critical points [HH89]; it is also used to define critical points in [BHJ16]. According to the following relation,

$$\nabla_{x'} x \overset{(5)}{=} \nabla_{x'}(Q^T(t)(x - r(t))) = Q^T(t), \qquad (14)$$

the Jacobian behaves under transformations (5) via

$$J'(x',t) \overset{(13)}{=} \nabla_{x'} v'(x',t)$$
$$\overset{(8)}{=} \nabla_{x'}(\dot{Q}(t)x + Q(t)v(x,t) + \dot{r}(t))$$
$$\overset{(14)}{=} \dot{Q}(t)Q^T(t) + Q(t)\nabla_x v(x,t)Q^T(t) \qquad (15)$$
$$\overset{(13)}{=} \dot{Q}(t)Q^T(t) + Q(t)J(x,t)Q^T(t),$$

making it not objective, but Galilean invariant.

5.1.5. Material Derivative of the Jacobian (Unsteadiness)

Unsteadiness [FKS*10] is the material derivative of the Jacobian

$$\frac{D}{Dt}J(x,t) \overset{(13)}{=} \frac{D}{Dt}\nabla_x v(x,t) = \nabla_x \frac{D}{Dt}v(x,t) \overset{(11)}{=} \nabla_x a(x,t). \quad (16)$$

The derivative transforms via

$$\frac{D}{Dt}J'(x',t) \overset{(16)}{=} \nabla_{x'} a'(x',t)$$
$$\overset{(12)}{=} \nabla_{x'}(\ddot{Q}(t)x + 2\dot{Q}(t)v(x,t) + Q(t)a(x,t) + \ddot{r}(t))$$
$$\overset{(14)}{=} \ddot{Q}(t)Q^T(t) + 2\dot{Q}(t)v(x,t)Q^T(t) + Q(t)a(x,t)Q^T(t),$$
$$\qquad (17)$$

which makes it Galilean invariant, but not objective.

5.1.6. Flow Map

A flow field can be given by both a vector field

$$\mathbb{R}^d \times \mathbb{R} \to \mathbb{R}^d, \quad x,t \mapsto v(x,t) \qquad (18)$$

and a flow map

$$\mathbb{R} \times \mathbb{R} \times \mathbb{R}^d \to \mathbb{R}^d, \quad t_0 \times t_1 \times x_0 \mapsto F_{t_0}^t(x_0), \qquad (19)$$

with

$$F_{t_0}^{t_0}(x_0) = x_0,$$
$$F_{t_1}^{t_2}(F_{t_0}^{t_1}(x_0)) = F_{t_0}^{t_2}(x_0). \tag{20}$$

The flow map describes how a flow parcel at (x_0, t_0) moves to $F_{t_0}^{t_1}(x_0)$ in the time interval $t_1 - t_0$.

These two representations are related through the initial value problem [Cod12],

$$\dot{F}_{t_0}^{t}(x_0) = v(F_{t_0}^{t}(x_0), t), \quad F_{t_0}^{t_0}(x_0) = x_0; \tag{21}$$

and inversely through

$$x_0 + \int_{t_0}^{t} v(F_{t_0}^{t}(x_0), t) dt = F_{t_0}^{t}(x_0). \tag{22}$$

The flow transforms like the spatial coordinates under (5)

$$
\begin{aligned}
F'_{t_0}^{t_1}(x_0') &\overset{(22)}{=} x_0' + \int_{t_0}^{t_1} v'(F'_{t_0}^{t_1}(x_0'), t) dt \\
&\overset{(8)}{=} x_0' + \int_{t_0}^{t_1} \dot{Q}(t) F_{t_0}^{t_1}(x_0) + Q(t) \dot{F}_{t_0}^{t_1}(x_0) + \dot{r}(t) dt \\
&= x_0' + \int_{t_0}^{t_1} \dot{Q}(t) F_{t_0}^{t_1}(x_0) dt + \int_{t_0}^{t_1} Q(t) \dot{F}_{t_0}^{t_1}(x_0) dt + [r(t)]_{t_0}^{t_1} \\
&\overset{\text{integration by parts}}{=} x_0' + [Q(t) F_{t_0}^{t_1}(x_0) + r(t)]_{t_0}^{t_1} \\
&= x_0' + Q(t_1) F_{t_0}^{t_1}(x_0) + r(t_1) - (Q(t_0) F_{t_0}^{t_0}(x_0) + r(t_0)) \\
&\overset{(5)}{=} x_0' + Q(t_1) F_{t_0}^{t_1}(x_0) + r(t_1) - x_0' \\
&= Q(t_1) F_{t_0}^{t_1}(x_0) + r(t_1).
\end{aligned}
\tag{23}
$$

Equation (23) means that the flow map is neither objective nor Galilean invariant.

5.1.7. Distance Between Particles

The distance between particles living in the same time frame is objective because of the length preservation of orthogonal transformations:

$$
\begin{aligned}
&\| F'_{t_0}^{t_1}(x_0') - F'_{t_0}^{t_1}(y_0') \| \\
&\overset{(23)}{=} \| Q(t_1) F_{t_0}^{t_1}(x_0) + r(t_1) - Q(t_1) F_{t_0}^{t_1}(x_0) + r(t_1) \| \\
&= \| Q(t_1)(F_{t_0}^{t_1}(x_0) - F_{t_0}^{t_1}(x_0)) \| \\
&= \| F_{t_0}^{t_1}(x_0) - F_{t_0}^{t_1}(x_0) \|.
\end{aligned}
\tag{24}
$$

The distance is inversely correlated to particle density [WCW*11].

5.1.8. Deformation Gradient

The deformation gradient [MW99, HFB*17]

$$\mathbb{R} \times \mathbb{R} \times \mathbb{R}^d \to \mathbb{R}^{d \times d}, \quad t_0 \times t_1 \times x_0 \mapsto \nabla F_{t_0}^{t_1}(x_0) \tag{25}$$

transforms via

$$
\begin{aligned}
\nabla_{x_0'} F'_{t_0}^{t_1}(x_0') &\overset{(23)}{=} \nabla_{x_0'}(Q(t_1) F_{t_0}^{t_1}(x_0) + r(t_1)) \\
&= Q(t_1) \nabla_{x_0'} F_{t_0}^{t_1}(x_0) \\
&\overset{(14)}{=} Q(t_1) \nabla_{x_0} F_{t_0}^{t_1}(x_0) Q(t_0)^T
\end{aligned}
\tag{26}
$$

because of the chain rule [Liu03], which means that the deformation gradient is not objective, but Galilean invariant.

On the other hand, the determinant of the deformation gradient is objective, due to the multiplicativity of the determinant and the orthogonality of $Q(t)$:

$$|\nabla F'| = |Q(t_1) \nabla F Q^T(t_0)| = |Q(t_1)||\nabla F||Q^T(t_0)| = |\nabla F|. \tag{27}$$

5.1.9. Cauchy Green Strain Tensor

The right Cauchy-Green strain tensor

$$
\begin{aligned}
&\mathbb{R} \times \mathbb{R} \times \mathbb{R}^d \to \mathbb{R}^{d \times d}, \\
&t_0 \times t_1 \times x_0 \mapsto C_{t_0}^{t_1}(x_0) = (\nabla F_{t_0}^{t_1}(x_0))^T \nabla F_{t_0}^{t_1}(x_0)
\end{aligned}
\tag{28}
$$

and its eigenvalues are the basis for the the finite-time Lyapunov exponent (FTLE) [Hal02b] and related methods based on particle expansion and contraction [SW10, USE12, BDBR*19, BDZG19]. The tensor transforms via

$$
\begin{aligned}
C'_{t_0}^{t_1}(x_0') &\overset{(28)}{=} (\nabla F'_{t_0}^{t_1}(x_0'))^T \nabla F'_{t_0}^{t_1}(x_0') \\
&\overset{(26)}{=} (Q(t_1) \nabla F_{t_0}^{t_1}(x_0) Q(t_0)^T)^T Q(t_1) \nabla F_{t_0}^{t_1}(x_0) Q(t_0)^T \\
&= Q(t_0)(\nabla F_{t_0}^{t_1}(x_0)^T \nabla F_{t_0}^{t_1}(x_0)) Q(t_0)^T \\
&\overset{(28)}{=} Q(t_0) C_{t_0}^{t_1}(x_0) Q(t_0)^T.
\end{aligned}
\tag{29}
$$

Its eigenvalues do not change if an orthogonal matrix is multiplied

$$
\begin{aligned}
\lambda(C'_{t_0}^{t_1}(x_0')) &\overset{(29)}{=} \lambda(Q(t_0) C_{t_0}^{t_1}(x_0) Q(t_0)^T) \\
&= \lambda(C_{t_0}^{t_1}(x_0)),
\end{aligned}
\tag{30}
$$

which makes them objective.

5.1.10. Distance Between Particles in Different Times

The displacement field [WRT18]

$$\mathbb{R} \times \mathbb{R} \times \mathbb{R}^d \to \mathbb{R}^d, \quad t_0 \times t_1 \times x_0 \mapsto d_{t_0}^{t_1}(x_0) = F_{t_0}^{t_1}(x_0) - x_0 \tag{31}$$

depending on the start location x_0, start time t_0, and end time t_1, measures the distance between particles observed at different times. To each start point x_0, it assigns the vector between it and the later location of a flow parcel that was released at time t_0 at location x_0. The displacement field transforms via

$$
\begin{aligned}
d'_{t_0}^{t_1}(x_0') &\overset{(31)}{=} F'_{t_0}^{t_1}(x_0') - x_0' \\
&\overset{(23)}{=} Q(t_1) F_{t_0}^{t_1}(x_0) + r(t_1) - (Q(t_0) x_0 + r(t_0)) \\
&= Q(t_1)(F_{t_0}^{t_1}(x_0 - x_0) + (Q(t_1) - Q(t_0)) x_0 + r(t_1) - r(t_0) \\
&\overset{(31)}{=} Q(t_1) d(x_0, t_0, t_1) + (Q(t_1) - Q(t_0)) x_0 + r(t_1) - r(t_0),
\end{aligned}
\tag{32}
$$

which makes it neither objective nor Galilean invariant.

5.2. Counter Examples and Theorems

We now provide a collection of mini counter examples and theorems to infer whether certain concepts generally satisfy one of the desired properties (Sec. 2.2) or not. These examples are tailored toward specific papers that we classify in Sec. 4 and therefore do not form a comprehensive narrative. This section is best read non-linearly using Tables 1– 4 as a road map. For better orientation, the following subsections are named in accordance with the four approaches and the tables that they belong to.

5.2.1. Tracking of Steady Topology

This subsection contains counter examples for Table 1.

Example 1 The classical steady vector field topology is not Langrangian; its critical points, especially, do not form pathlines. As a counter example, we look at the 1D vector field

$$v(x,t) = x + t - 1. \tag{33}$$

This field has a classical critical point at $x_0(t) = 1 - t$. This critical point does not form a pathline, because it is not tangential to the vector field $v(x_0(t),t) = 1 - t + t - 1 = 0 \neq \dot{x}_0(t) = -1$.

Example 2 The classical steady vector field topology is not Galilean invariant. As a counter example, we look at the 1D steady vector field

$$v(x,t) = x. \tag{34}$$

$v(x,t)$ transforms under the Galilean coordinate transform $x' = x + t$ to the field (33). Its critical point at $x_0(t) = 0$ transforms to $x'_0(t) = t$, which does not coincide with the critical point at $1 - t$ of the transformed field (33).

5.2.2. Reference Frame Adaption

This subsection contains counter examples for Table 2.

Theorem 1 The localized flows that correspond to the diverging and rotating parts of the Helmholtz-Hodge decomposition from Wiebel *et al.* [WGS02] and from Bhatia *et al.* [BPB14, BPKB14] are Galilean invariant.

Proof Assume a vector field $v(x,t) : \mathbb{R}^d \times \mathbb{R} \to \mathbb{R}^d$ that has the Helmholtz Hodge decomposition

$$v(x,t) = d(x,t) + r(x,t) + h(x,t) \tag{35}$$

with d containing the divergent part, r the rotational part, and h the harmonic part. It follows from (8) that the transformed field by a time-dependent translation $x' = x + r(t)$ has the form

$$v'(x',t) = v(x,t) + \dot{r}(t) \tag{36}$$

Since $\dot{r}(t)$ is independent of x, it is divergence and rotation free and belongs to the harmonic part h of the decomposition. As a result, it has no influence on the localized flows suggested by both methods $v^*(x,t) := d(x,t) + r(x,t)$ where the harmonic part is removed. □

Example 3 If the steady vector field topology is applied to the localized flows that correspond to the diverging and rotating parts of the Helmholtz-Hodge decomposition from Wiebel *et al.* [WGS02] and from Bhatia *et al.* [BPB14, BPKB14], the result does not generally coincide with the steady case. Theorem 1 shows that adding a constant to a vector field leaves the localized flow unchanged, but it moves the locations of the classical topology.

Example 4 The decomposition by Wiebel *et al.* [WGS02] is not objective. Assume a 2D vector field that has vanishing outflow on a circular boundary. A rotation around the center of the coordinates leaves the outflow zero, which means the decomposition leaves the field unchanged, and the result of Wiebel's algorithm is identical to the input. If we apply the classical topology, then it follows from the velocity (8) that the result is not objective.

Example 5 We show that the method by Bhatia *et al.* [BPB14, BPKB14] is not objective for the example of the zero vector field

$$v(x,y) = \begin{pmatrix} 0 \\ 0 \end{pmatrix}. \tag{37}$$

Its localized flow $v^*(x_0,y_0) = d^*(x_0,0) + r^*(x_0,0)$ is also zero, because

$$\begin{aligned} D^*(x_0,y_0) &:= \int_\Omega G_\infty(x,x_0) \nabla \cdot v(x) dx = 0, \\ R^*(x_0,y_0) &:= -\int_\Omega G_\infty(x,x_0) \nabla \times v(x) dx = 0, \end{aligned} \tag{38}$$

where G_∞ is the free-space Green's function, and

$$\begin{aligned} d^*(x_0,y_0) &:= \nabla \cdot D^*(x_0) = 0, \\ r^*(x_0,y_0) &:= \nabla \times R^*(x_0) = 0. \end{aligned} \tag{39}$$

It follows from (8) that the rotated counterpart by $x' = Q(t)x$ with the matrix representing a rotation by πt at time $t = 0$ suffices

$$\tilde{v}(x,t) = \begin{pmatrix} -y \\ x \end{pmatrix}. \tag{40}$$

In the Helmholtz Hodge decomposition, this part must be in the rotational component, because it is not harmonic nor divergent. Therefore, the rotational part does not coincide with its original counterpart, which was zero.

Example 6 We show that the Helmholtz-Hodge decomposition from Wiebel *et al.* [WGS02] and from Bhatia *et al.* [BPB14, BPKB14] is not Lagrangian.

For example, if we decompose a vector field with vanishing outflow on the boundary, the Helmholtz-Hodge decomposition in Wiebel *et al.* [WGS02] returns the original field back. Therefore, a slight variation of Example 1 can be used to show that the method is not Lagrangian.

Assume a steady vector field that is zero outside the unit ball $\forall |x| > 1 : v(x) = 0$, has no harmonic part and a critical point $x_0 \neq 0$. The unsteady field that we get from rotating it around the origin also has no outflow and no harmonic part and is therefore not changed by either of the two methods. Its critical points are not Lagrangian, similar to Example 1.

Theorem 2 The steadification by Hadwiger *et al.* [HMTR18] coincides with the steady case if the regularization term is omitted, i.e. for $\mu = 0$.

Proof Setting $\mu = 0$ reduces the energy term $E = E_K + \lambda D_t + \mu R$ that is minimized globally to $E = E_K + \lambda D_t$, where E_K is the Killing energy of the coordinate transform u and D_t is the temporal derivative of the output field v_u. The temporal derivative of a steady input field $v : \mathbb{R}^d \to \mathbb{R}^d$ is zero $D_t = 0$ and the Killing energy of the identity transform $u = 0$ is zero, too, $E_K = 0$. If the regularization is omitted, then the overall energy of $v_u = v, u = 0$ is $E = E_K + D_t = 0$, which makes it the minimum. □

Example 7 We will show that the method suggested by Hadwiger *et al.* [HMTR18] does not generally leave steady fields unchanged for positive regularization weights $\mu > 0$. For simplicity, we assume that the steady 1D vector field

$$v(x) = x \tag{41}$$

is transformed via a Galilean transformation $x' = x - ct$ only. Then the transforming field is a Killing field $u(x,t) = c$ satisfying

$$x' = x - \int_0^t u(x(\tau),\tau)d\tau = x - \int_0^t cd\tau = x - ct \qquad (42)$$

and the transformed field takes the shape

$$v'(x',t) = v(x) - u(x,t) = x - c = x' + ct - c. \qquad (43)$$

Then, since u is Killing, the Killing energy does not contribute to the energy integral. We assume $\lambda = 1, \mu = 2$ and the domain $\Omega = [0,1] \times [-1,1]$. Then the energy has the form

$$\begin{aligned} E(c) &= \int_0^1 \int_{-1}^1 |\frac{Dv_u(\xi,\tau)}{Dt}| + 2|v_u(\xi,\tau)|d\tau d\xi \\ &= \int_0^1 \int_{-1}^1 |v_t + \nabla v \cdot u| + 2|x + ct - c|d\tau d\xi \qquad (44) \\ &= \int_0^1 \int_{-1}^1 |0 + 1c| + 2|x + ct - c|d\tau d\xi, \end{aligned}$$

which takes its minimum at $E(-3/16) = 29/16$, which means, the steady field $v(x) = x$ is transformed into the unsteady field $v_u(x,t) = x - 3/16t + 3/16$. As a result, applying the steady topology to the adapted field v_u does in general not coincide with the steady topology of the input field.

It follows from Theorem 2 that this effect is a consequence of the regularization. It can be mitigated with a small change:

1. Try to compute the observer field with $\mu = 0$, i.e. disabling the regularization. If a unique minimum is found, the corresponding observer field will leave steady fields unchanged.
2. If there was no unique minimum, set μ to a very small value and compute the observer field with that.

Example 8 We will show that the critical lines in the steadified field as produced by the method suggested by Hadwiger *et al.* [HMTR18] are not generally Lagrangian. For simplicity, we assume $\mu = 0$ and $0 < \lambda << 1$, i.e. the weights are set such that the Killing energy term in the minimization is weighted unproportionally high so that only true Killing fields u are possible and the energy minimization only concerns the steadiness. Analogously to Example 7, we treat a 1D vector field

$$v(x) = (x - t^2)^2 \qquad (45)$$

under only a Galilean transformation $x' = x - ct$

$$v'(x',t) = v(x) - u(x,t) = (x - t^2)^2 - c = (x' + ct - t^2)^2 - c. \qquad (46)$$

Over the domain $\Omega = [0,1] \times [-1,1]$ the energy takes the form

$$E(c) \stackrel{(44)}{=} \lambda \int_0^1 \int_{-1}^1 |4t(-t^2 + x) - c(2x - 2t^2)|d\tau d\xi, \qquad (47)$$

which takes its minimum at $E(0) = 4/3$. That means, the input field is not transformed. Its zeros are $x_0(t) = t^2$ with tangent $\dot{x}_0(t) = 2t$ not pointing in the direction of the flow $v_u(x_0(t),t) = 0$.
Since pathlines are transformed into pathlines through the transformation, the line $x_0(t)$ transformed into the original coordinates is also not a pathline in the original field.

Example 9 We show that the optimization suggested by Rojo *et*

al. [RG20] does not generally extract Lagrangian critical points. As an example, we take the vector field

$$v(x,t) = \binom{(x - t^2)^2}{y^2} \qquad (48)$$

We assume a Galilean transformation that does not depend on space, so the zeroth order Taylor approximation of the displacement function should be sufficient. In that case, the matrix M has the shape

$$M(x,t) = (-J \quad I) = \begin{pmatrix} 2t^2 - 2x & 0 & 1 & 0 \\ 0 & -2y & 0 & 1 \end{pmatrix}, \qquad (49)$$

The partial temporal derivative of v suffices

$$v_t(x,t) = \binom{4(t^2 - x)t}{0}, \qquad (50)$$

For each location, we integrate over a symmetric spatial neighborhood $[-c,c]^2$ and solve the least squares fit

$$\int_{-c}^c \int_{-c}^c M^T(x,t)M(x,t)dxdy \, p = -\int_{-c}^c \int_{-c}^c M^T v_t dxdy, \qquad (51)$$

which results in

$$p = \begin{pmatrix} -2t \\ 0 \\ 0 \\ 0 \end{pmatrix} \qquad (52)$$

independently of the location and neighborhood size.
As a result, the steadified flow w takes the form

$$w(x,t) = v(x,t) + \binom{-2t}{0} = \binom{(x - t^2)^2 - 2t}{y^2}. \qquad (53)$$

Its zeros are located at $x_0^w(t) = (t^2 \pm \sqrt{2t}, 0)$ with tangent $\dot{x}_0^w(t) = (2t \pm 1/\sqrt{2t}, 0)$. The vector fields f and v point along $v(x_0^w(t),t) = (2t,0)$ though, which means that $x_0^w(t)$ is not a pathline. Therefore, the method is not Lagrangian.

5.2.3. Categorize/Cluster Pathlines

This subsection contains counter examples for Table 3.

Example 10 We illustrate that the pathline-oriented topology by Theisel *et al.* [TWHS04, TWHS05] is not Galilean invariant using a 1D vector field

$$v(x,t) = \begin{cases} x, & \text{if } t = 0, \\ -1, & \text{if } t > 0, \\ 1 & \text{if } t < 0 \end{cases} \qquad (54)$$

defined on a grid with cell size 1. A visualization can be found in Fig. 14. The point $x_0 = 0$ will be classified as a source by the pathline-based topology from [TWHS04, TWHS05], because the plane in spacetime orthogonal to $v(0,0) = 0$, is just the time slice itself, and the neighboring points in this plane are $(-1,0)$ and $(1,0)$, which have expanding character $v(-1,0) = -1$ and $v(1,0) = 1$. Now we transform the vector field through the Galilean transformation $x' = x - t$. It follows from (8) that

$$v(x,t) = \begin{cases} x - 1, & \text{if } t = 0, \\ -2, & \text{if } t > 0, \\ 0 & \text{if } t < 0. \end{cases} \qquad (55)$$
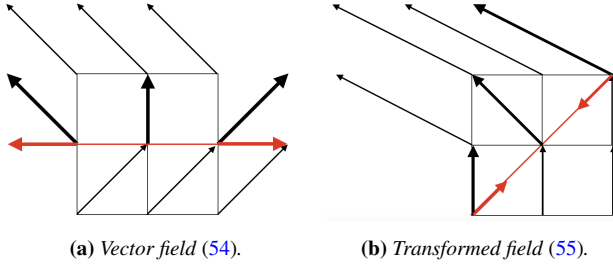
(a) *Vector field* (54). **(b)** *Transformed field* (55).

Figure 14: *An example 1D vector field (time vertical, space horizontal) that shows that the pathline-oriented topology by Theisel et al. [TWHS04, TWHS05] is not Galilean invariant. The source is transformed into a sink through the transformation. The red line shows the plane orthogonal to the velocity and the red arrows the projections on the plane.*

(a) *Velocity of the 1D vector field $v(x)$ from* (56). **(b)** *Its flowmap $F_0^1(x_0)$ from* (57) *visualized through endpoint as function of startpoint.* **(c)** *Flowmap gradient $\nabla F_0^1(x_0)$ from* (58) *and 1 as reference to separate expanding from attracting regions.*

Figure 15: *The maximum expansion $x \in [0.5, 1.55e^{-t} + 0.45]$ and the saddle location $x = 0$ do in general not coincide. Horizontal axis: space.*

Here, at $t = 0$, the point $x_0' = 0$ will be classified as a sink. Its neighboring points in the plane orthogonal to $v(0,0) = -1$ are $(-1,-1)$ and $(1,1)$. Their vectors in spacetime projected on this plane take the shape $v'(-1,-1) = 1/2$ and $v'(1,1) = -1/2$, which makes them contracting.

Example 11 In this example, we will demonstrate that the locations of the strongest expansion or contraction of the flowmap as used, for example, in [SW10, WCW*11, USE12, BDZG19], will in general not coincide with the critical points in a steady field. To illustrate our idea, we use a 1D example, in which all particles starting in $(0, 3.55)$ move to the right toward 3.55,

$$v(x) = \begin{cases} 0.1x, & \text{if } x \in (0, 0.5] \\ x - 0.45, & \text{if } x \in (0.5, 2] \\ 3.55 - x, & \text{if } x \in (2, 3.55]. \end{cases} \quad (56)$$
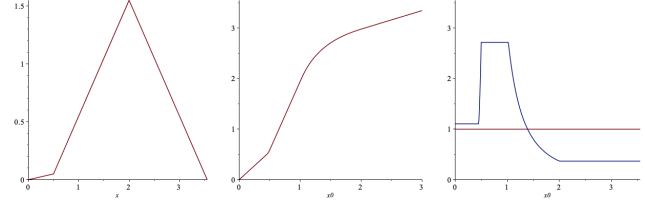
The flowmap of (56) takes the form

$$F_0^t(x_0) = \begin{cases} x_0 e^{0.1t}, & \text{if } x_0 \in (0, 0.5e^{-0.1t}) \\ 0.9 - 51.2x_0^{10}e^t, & \text{if } x_0 \in [0.5e^{-0.1t}, 0.5] \\ 0.9 + e^t(x0 - 0.9), & \text{if } x_0 \in [0.5, 1.55e^{-t} + 0.45] \\ \frac{3.55 - 1.55e^{-t}}{1.55x_0 - 0.45}, & \text{if } x_0 \in [1.55e^{-t} + 0.45, 2] \\ 3.1 + e^{-t}(x0 - 3.1), & \text{if } x_0 \in (2, 3.55] \end{cases}$$
$$(57)$$

for integration times small enough that no particle crosses both boundaries $x = 0.5$ and $x = 2$ between the different cases in (56), which is true for $t < 3.43$, especially for the case of $t = 1$ that we will look at.
The gradient of the flowmap (57) suffices

$$\nabla F_0^t(x_0) = \begin{cases} e^{0.1t}, & \text{if } x_0 \in (0, 0.5e^{-0.1t}) \\ 512x_0^9 e^t, & \text{if } x_0 \in [0.5e^{-0.1t}, 0.5] \\ e^t, & \text{if } x_0 \in [0.5, 1.55e^{-t} + 0.45] \\ \frac{1}{e^t(1.55x_0 - 0.45)^2}, & \text{if } x_0 \in [1.55e^{-t} + 0.45, 2] \\ e^{-t}, & \text{if } x_0 \in (2, 3.55] \end{cases}$$
$$(58)$$

The graphs of these functions for $t = 1$ can be found in Fig. 15. The maximum expansion is constant in the whole inter-

val $[0.5, 1.55e^{-t} + 0.45]$, which excludes the true location of the critical point at $x_0 = 0$.

5.2.4. Generalization of Critical Points

This subsection contains counter examples for Table 4.

Example 12 Kasten *et al.* [KHNH11] use locations that minimize the acceleration. Since in a steady field the acceleration in a critical point is zero, all classical critical points are included, i.e., the definition is *sufficient*. The following 1D example will show that the definition is not *necessary*, however.
The 1D vector field

$$v(x) = \sqrt{x} + xe^{-|x|} \quad (59)$$

has the acceleration

$$a(x) = (\frac{1}{2\sqrt{x}} + e^{-|x|} - \frac{x^2 e^{-|x|}}{|x|})(\sqrt{x} + xe^{-|x|}) \quad (60)$$

and an acceleration minimum around $x \approx 2.5$, which does not correspond to a critical point, Fig. 16.

Example 13 The lines of vanishing acceleration are in general not pathlines, for example, the 1D time-dependent vector field

$$v(x,t) = x + t^2 \quad (61)$$

has the acceleration

$$a(x,t) = t^2 + 2t + x \quad (62)$$

with a zero along the line $x_0(t) = -t^2 - 2t$. The tangent of this line satisfies $\dot{x}_0(t) = -2t - 2$, but the vector field along this line suffices $v(x_0(t), t) = -2t$, which means that it does not follow the line, which means that methods suggested by Kasten *et al.* [KHNH11] and Fuchs *et al.* [FKS*10], and the acceleration-based method by Reininghaus *et al.* [RH11] are not Lagrangian.
Kasten *et al.* [KHNH11] and Fuchs *et al.* [FKS*10] further their idea of looking for acceleration minima/zeros using Lagrangian smoothing and introduce Lagrangian equilibrium points, which are pathlines that exhibit low acceleration over a period of time. Their method relies on several parameters: thresholds for the acceleration, the relative acceleration compared to neighboring points, and a
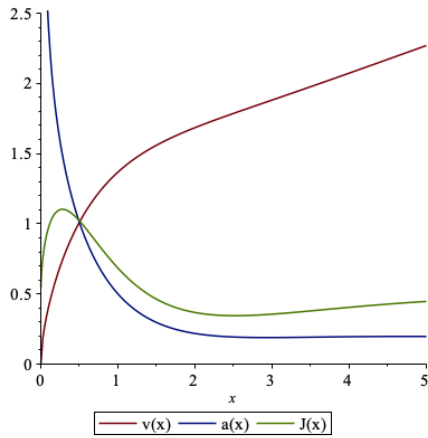
Figure 16: *The field* (59) *v is in red, its Jacobian J is in green, and its acceleration a is in blue. The acceleration assumes a minimum around $x \approx 2.5$ even though neither the Jacobian nor the velocity is zero there.*

(a) *Velocity magnitude of* (63) *shows the critical point at* $(1,0)$.

(b) *The determinant of the Jacobian has a maximum at* $(0,0)$.

Figure 17: *Example where the method by Bujack et al. [BDZG19] does not coincide with the steady case.*

time window. If the full time is used, then this method becomes Lagrangian, but the authors use a sliding window method. Therefore, the method is not Lagrangian, because of Section 2.3 in [Hal15].

Theorem 3 If the input field is steady and the locations of vanishing acceleration $a(x) = 0$ are nondegenerate, i.e., the Jacobian has full rank, $\det J(x) \neq 0$, the acceleration zeros coincide with the classical first-order critical points $v(x) = 0$.

Proof In the case of a steady vector field, the acceleration $a = \nabla v v + v_t$ simplifies to $a = \nabla v v$, which is zero iff $v = 0$ or the rank of ∇v is not full and v is in its kernel. In the former case, we have a steady critical point. In the latter case, the determinant of the Jacobian ∇v is zero, which would make it degenerate. $\square$

Example 14 Bujack *et al.* [BHJ16] look at extrema of the determinant of the Jacobian. These do not generally coincide with the classical critical points. For example, the steady vector field

$$v(x,y) = \begin{pmatrix} x-1 \\ y \end{pmatrix} e^{-\sqrt{x^2+y^2}} \tag{63}$$

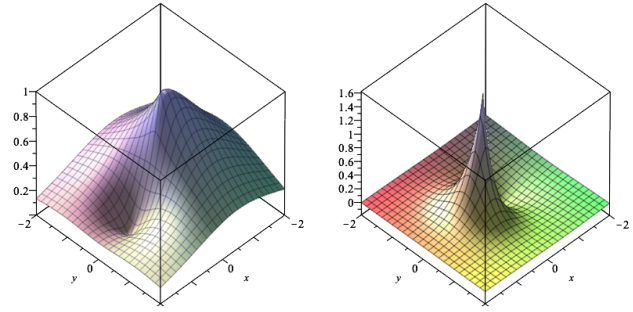has a critical point at $(1,0)^T$, but the maximum of the determinant of the Jacobian

$$e^{-2\sqrt{x^2+y^2}} \frac{\sqrt{x^2+y^2}(x^2+y^2-x)-x^2-y^2}{x^2+y^2} \tag{64}$$

is located at $(0,0)^T$, compare Fig. 17.

The same example shows that the method is not Lagrangian, because the tangent $\dot{x}_0(t) = (0,0)^T$ of the extracted line of maximum determinant of the Jacobian $x_0(t) = (0,0)^T$ is not tangential to the vector field $v(x_0(t)) = v(0,0) = (-1,0)^T$.

Example 15 In this example, we discuss the Galilean invariance and Lagrangianness of the method by Machado *et al.* [MBES16]. The basic idea of this method is Galilean invariant, because for the special case of a spacetime field, the condition of the vector field being parallel to the acceleration $v \parallel a$ is equivalent to $a = 0$. In this formulation, the method does not depend on the velocity and

the acceleration in Galilean invariant, Sec. (5.1.3). Further, if the algorithm actually achieves a minimum angle of zero everywhere, i.e., converges to the closest pathline, then the result is also Galilean invariant if the metric compares distance in the same time only. This observation follows from Sec. (5.1.7) and because pathlines and the acceleration transform in the same way under Galilean changes of the reference frame, see Sec. 5.1.6 and Sec. 5.1.3.

However, the algorithm in Machado *et al.* [MBES16] cannot guarantee this convergence to the corresponding pathlines, because it depends on the angle between the zero acceleration tangent and the vector field, which is not Galilean invariant. We illustrate such an observation using the example vector field (61). There the angle between the tangent of the line of zero acceleration and the vector field at $t = 0$ in phase space is $\angle((-2,1),(0,1)) = \arccos(sqrt(5)/5) \approx 1.11$. However, the transformed field

$$v'(x,t) = x - t + 1 + t^2 \tag{65}$$

has the acceleration

$$a'(x,t) = t^2 + t + x \tag{66}$$

has a zero along the line $x_0(t) = -t^2 - t$. The tangent there satisfies $\dot{x}_0(t) = -2t - 1$ and the vector field $v(x_0(t),t) = -2t + 1$. Therefore, the angle between the two at $t = 0$ in phase space is $\angle((-1,1),(1,1)) = \pi/2 \approx 1.57$.

Machado *et al.* [MBES16], in particular, filter out initial loci of zero acceleration based on a threshold if this angle is too big. If the threshold had, for example, been chosen to be 1.2, then the transformed field would have a candidate line for refinement that exists for $t = 0$, whereas the initial field would not.

In comprehension, even though the acceleration and its zeros are Galilean invariant, the angle between its tangent and the vector field are not. Therefore, the method by Machado *et al.* [MBES16] is not Galilean invariant, and it is especially not objective.

If the method does not converge to a pathline, the result is not Lagrangian and even if the initial loci locally converge to a pathline, they will not generally form complete pathlines. For example,

$$v(x,y,t) = \begin{cases} (x,-y)^T, & \text{if } t < 0, \\ t, \text{else.} \end{cases} \tag{67}$$

has zero acceleration in a hyperbolic region for all $(0,0,t)$ if $t < 0$, but the acceleration is constantly $a = 1$ and never zero for $t > 0$. The refinement does not change anything, because the tangent $(0,0,1)$ is already parallel to the vector field in spacetime $(0,0,1)$.

Example 16 The method by Wang *et al.* [WBPRH17] does not find a second critical point to cancel out a generalized critical point for the simple example (63). We will assume that, in this case, such a critical point cancels out with a fictional point at infinity. The field is so simple that, in order to reach infinity from each point in its own reference frame $\tilde{v}(x,y) = v(x,y) - v(x_0,y_0)$, we will find a monotonic path in the adapted velocity magnitude field. Therefore, we can get the robustness from the difference of the velocity magnitude of the point in question, which is zero in its own frame, and infinity, which is $\lim_{\sqrt{x^2+y^2} \to \infty} \|v(x,y) - v(x_0,y_0)\| = \|v(x_0,y_0)\|$. Therefore, the maximum of the generalized robustness is also located at $(0,0)$ like in Example 14. As a result, the method by Wang *et al.* [WBPRH17] does not coincide with the classical topology and is not Lagrangian.

6. Related Work Beyond Visualization

The study of time-dependent flow topology goes beyond visualization literature to include fluid dynamics and dynamical systems, to name a few. As the goal of visualization is to help application scientists gain insight into their data and amplify cognition [CMS99], we think paying close attention to their problems and solutions is crucial, because they have a deeper understanding of their field. Oftentimes advancements in mathematics, science, and engineering will inspire new visualization techniques. We provide some examples in this section that we think are most promising in advancing the topology and visualization of unsteady flow in the future.

The content in this section may be outside the comfort zone of a visualization researcher. However, we believe that advancements external to visualization, in particular, from fluid dynamics and dynamical systems, offer inspiring perspectives on flow topology. Practitioners may want to skip this section on their first reading.

6.1. Fluid Dynamics

In fluid dynamics, scientists often have a different approach to deal with the dependence of the instantaneous velocity on the frame of reference (FOR). For example, topological information is usually used to classify not only critical points but also the entire domain of a field, which overcomes the dependency on Galilean reference changes and allows a statistical evaluation [Can93, SSC*94, CCK96, CC00]. Scientists also often use a Reynolds decomposition to separate the flow into its *average* component and its deviation, where the average could be taken over time, over space, and over an ensemble.

Blackburn *et al.* and others [BMC96, CCK96, CSP*98] use the boundaries between regions with complex eigenvalues and regions with real eigenvalues to segment the domain into coherent regions. Chong *et al.* [CPC90] define critical points in 3D flow as points where the streamline slope is indeterminate and the velocity is zero relative to an appropriate observer. They classify streamlines based on their 2D behavior surrounding critical points in the three

eigenvector planes. They explicitly exclude rotating frames and assume the center of coordinates to follow a fluid particle. Soria *et al.* [SSC*94] compute the invariants of the Jacobian everywhere in the domain and detect a teardrop shape that seems characteristic for incompressible fluid flow. Later, Chacin and Cantwell [CC00] use the Lagrangian averaged invariants of the Jacobain along pathlines to detect two separate regions of high concentrations. They further find that boundaries between regions with complex eigenvalues and those with real eigenvalues correlate only with regions of high Reynolds stress and kinetic energy generating events.

Ide *et al.* [ISW02] analyze distinguished hyperbolic trajectories. They consider a trajectory *hyperbolic* if the linearization of the flow about it has a full set of exponentially growing or decaying solutions. A trajectory is *distinguished* if it resides in a bounded neighborhood for all time while all its neighbors leave this neighborhood. If all trajectories leave the domain, Ide *et al.* apply a coordinate transformation based on a Eulerian structure, like a critical point. They show that there are no unique distinguished hyperbolic trajectories if the flow field is given for only a finite time, but suggest an approximation based on an artificial extension of the time to infinity using the Fourier series. They show that these trajectories match the expected critical lines in linear fields even under reference frame changes. Later Ju *et al.* [**?**] suggest an iterative algorithm for the computational extraction of these approximate distinguished hyperbolic trajectories. Branicki and Wiggins [BW09] extend the iterative algorithm to three-dimensional flow.

6.2. Almost Invariant Sets

First, we include some literature on alternative formulations of steady vector field topology based on *almost invariant sets* that arise from dynamical systems.

In the visualization literature, vector field topology is mostly defined as a segmentation of the domain into regions of equivalent (or uniform) streamline behavior in terms of "start" and "end" sets.

An alternative formulation that provides a Morse segmentation of the domain is based on the notion of *isolating invariant sets* and *isolating sets*. These sets can be classified according to their Conley index, which corresponds to the Poincaré index for critical points. At least in the case of 2D vector fields, the resulting segmentation is closely related to the standard approach. This formulation has the advantage that it can be more easily generalized to a discrete setting, as is common for real-world flow data. The formulation, therefore, gives rise to more robust computation in extracting topological skeleton.

In this setting, the flow could be interpreted as a mapping from a temporal discretization of a vector field. Given a steady vector field v on a domain X, the map $f : X \to X$ describes the movement from one time step t to the next time step $t + \tau$. A trajectory through a point $x \in X$ is then a function $\sigma_x : Z \to X$ generated by consecutive application of the function f, with $\sigma_x(0) = x$ and $\sigma_x(n+1) = f(x(n)) = f^k(x)$. In conjunction with a spatial discretization, the vector field can then be represented using a transfer operator and given as a transfer matrix. There is an inherent numerical diffusion associated with the discretization procedure, and the

notion of invariant sets is replaced by *almost invariant sets*. For example, based on this formulation, closed orbits are represented by ε-chain recurrent sets. Critical points are examples for isolating invariant sets and can be represented by isolating neighborhoods that are robust with respect to small changes in the field.

This concept provides the basis for several algorithmic approaches for the extraction of the dynamic structures of a vector field by computing an "optimal" decomposition into almost invariant sets. These are computational methods that can provide accurate information about global structures of nonlinear dynamical systems and are rigorous in the sense of mathematical proofs [Mis02, CMLZ08]. Froyland *et al.* [Fro01, FD03] model the behavior of the dynamical system as a finite state Markov chain represented by a transition matrix. Their goal is to partition the phase space into a finite number of connected sets A_i with nonempty interior covering the phase space, which reveal the coarse-grained dynamics displayed by the evolution of the sets. They describe a numerical algorithm to detect "near-optimal almost-invariant sets and cycles". With respect to the standard vector field theory, their theory assumes a time-independent vector field and is neither Lagrangian nor Galilean invariant.

Second, we discuss the generalization of invariant sets to time-dependent vector fields, which then produce Lagrangian and objective features. An attempt to generalize this formulation to the time-dependent setting introduces time-coherent sets that relate sets in different time steps. The goal is to find coherent pairs of subsets $A_t, A_{t+\tau} \subset X$ such that $\phi(A_t, \tau) \simeq A_{t+\tau}$, where ϕ is the flow map and X is the domain or phase space. Since there is no obvious generalization of the property of being (almost) invariant, the main challenge is to define concise criteria when a time-coherent set qualifies as a topological feature. Several different criteria have been proposed in the literature, ranging from shape coherence to stability under perturbation. Froyland *et al.* [Fro12, FSM10] propose to define *finite-time coherent sets* as minimally dispersive and maximally coherent sets over finite periods of time. Their theory is built around the Multiplicative Ergodic Theorem. More specifically, they study pairs of sets that remain coherent under small diffusive perturbations of the flow. For a given sequence of maps $T_i : X \to X$, which represent a dynamical system, these are pairs of sets $A_t, A_{t+\tau} \subset X$ where $A_t \cap T^{-1}(A_t, \tau)$ is large. Probabilistic methods are proposed that automatically detect such maximally coherent sets. This condition favors coherent sets that are geometrically regular.

Based on such observations, Ma *et al.* [MB14] extract coherent sets by analyzing the change of the set boundaries when advecting the sets. The concept of coherent sets is based on transport properties of the flow and thus has a Lagrangian perspective. Since its computation is based only on the development of sets, it is also Galilean invariant and objective. The specifically chosen discretization, however, can violate the strict invariant condition.

6.3. Lagrangian Coherent Structures

Haller [Hal15] surveys the recent work on Lagrangian coherent structures (LCSs), in which he rejects his earlier approaches based on FTLE [HY00, Hal00, SLM05] and promotes lines and stretch lines as LCSs [FH12, FH13].

A survey that follows a similar structure as ours by Hadjighasem [HFB*17] analyzes and compares approaches to identify LCSs. He also analyzes the methods based on their mathematical properties. We briefly point out the most promising and least commonly used approaches for the field of visualization.

Froyland [Fro13, FPG14] follows the goal of identifying barriers to mixing, which are locally the strongest repelling or attracting objects. Central to the method is the analysis of the transfer operator, which is a linear operator providing a global description of the action of the flow on densities. In the implementation, this operator is discretized resulting in a Markov chain transition matrix. Almost invariant sets then correspond to singular vectors of this matrix.

Hadjighasem *et al.* [HKTH16] construct a similarity matrix $W \in \mathbb{R}^{n \times n}$ in which each entry W_{ij} is the reciprocal of the L^1 distances between the i-th and j-th particle trajectory. Then, they make use of spectral clustering to identify the optimal numbers of clusters by looking for the greatest difference between consecutive generalized eigenvalues in the matrix $D - W$, where D is the diagonal matrix that contains the row sums of W. Then, they use k-means to cluster the matrix $U \in \mathbb{R}^{n \times k}$ of the first generalized eigenvectors into $k + 1$ clusters, the additional one representing the incoherent background.

The geodesic theory of LCSs combines hyperbolic and parabolic LCSs, trajectories of average Lagrangian shear [FH12, FH13], and elliptic LCSs, closed trajectories of average strain [HBV13].

Banisch and Koltai [BK17] apply diffusion maps to cluster trajectories. Heil *et al.* [HRHB17] define flow topology through the scalar topology of the vorticity field. This notion of topology is applied to the Karman vortex street for different Reynolds numbers to better understand the formation of vortices. Rypina *et al.* [RSPB11] partition the domain concerning different levels of complexity (ergodicity, spatial coverage). Algorithmically, the number of sampling points on the pathline in cells is counted. The cell size is an algorithmic parameter. A pathline is considered as a fixed point if it is a minimum in the ergodicity field.

Mancho *et al.* [MWCM13] propose a Lagrangian descriptor for time-dependent dynamical systems. The main descriptor is based on the "finite-time length of particle trajectories". "Abrupt changes" in the length are related to region boundaries. The goal is to reveal and understand the organizing structures in phase space.

7. Future Research Opportunities

The aim of this paper is to identify challenges and opportunities in the study of time-dependent flow topology. A few avenues deserve further exploration.

7.1. Applications, Effectiveness, and Comprehensiveness

The desirable properties, their definitions and interpretations are a first attempt and probably not a perfect one to ensure general physical meaningfulness of flow topology in all related application fields. We see potential for extensions and evaluations in close collaboration with application scientists. Many topology extraction and visualization methods exist but there is not much information about which of them are truly effective in practice, and for which tasks.

There is a lack of studies that link such methods to concrete tasks, which is a big concern for practitioners. A big research opportunity, in our opinion, is to study related work outside the field of visualization, by understanding application-specific advancements and challenges (Sec. 6).

Inspecting the summary of our results in Tables 1 – 4, we clearly see that, currently, no technique is comprehensive (i.e., it satisfies all properties). The mathematical foundations associated with the discussed properties, in particular, their assets and limitations, may be used to build novel techniques for time-varying flows. For instance, we consider the reference frame adaption (Sec. 4.2) and the categorization of pathlines (Sec. 4.3) to be the most promising ones to be made comprehensive. Maybe there are ways to combine the strengths of these two approaches to generate new ones.

7.2. Uncertainty Visualization

A major opportunity in topology-based visualization, as pointed out by Heine *et al.* [HLH*16b], is the incorporation of uncertainty.

For uncertain scalar fields, Mihai and Westermann [MW14] capture the likelihood of the occurrences of critical points, with respect to their positions and types across an ensemble. Hüttenberger *et al.* [HHC*13] use Pareto optimality to predict the positions of local extrema for multifield data. Günther *et al.* [DJJ14] introduce mandatory critical regions. Favelier *et al.* [FFST19] visualize positional uncertainties of critical points using persistence-based clustering.

For uncertain vector fields, Pfaffelmoser *et al.* [PMW13] analyze the variability in gradient fields induced by uncertain scalar fields. Otto *et al.* [OGHT10,OGT11] introduce Monte Carlo gradient sampling for visualizing variations of pathlines in 2D and 3D uncertain vector fields. Bhatia *et al.* [BJB*12] employ *edge maps* for the error analysis of uncertain gradient flows. Nagraj *et al.* [NNN11] propose a measure to quantify gradient uncertainty for multifield data.

For topological structures, various techniques are used to explore structural variations of contour trees [Kra10,WZ12,ZAM15], merge trees [YWM*20], and Morse–Smale complexes [TLB*11, AMJ*19]. Topological features, in particular, level sets, appear frequently in uncertainty visualization, including contour boxplots [WMK13], probabilistic marching cubes [PWH11, PH13], and their extraction from uncertain data [AE13, ASE16, AJ19].

Despite existing works in visualizing uncertainty for scalar fields, time-independent vector fields, and topological structures, capturing time-dependent flow topology in the face of uncertainty remains a largely unexplored area. The question is, given an ensemble of time-dependent flows, can we quantify and visualize the topological uncertainty of its ensemble members? By uncertainty, we mean information about the accuracy, confidence, and variability of their time-dependent topology.

7.3. Scalable Computation and Visualization

Scalability in scientific visualization is becoming crucial as the amount of data grows exponentially due to exascale computing [HCJ*14]. The availability of scalable, general purpose, and in situ visualization tools such as ParaView [FMT*11] and the Visualization Toolkit (VTK) [SML06] has greatly advanced the field. To find applications in cutting-edge simulations on supercomputers, newly developed methods must be able to run on GPUs, in distributed environments, or *in situ*.

Significant efforts that address the scalability issues have focused on scalable computations of topological structures such as contour trees [CWSA16, CWS*19], merge trees [MW13, SM17], and Morse–Smale complexes [SN12, SMN12]. Some works exist in the study of flow fields by applying clustering, sampling, distributed and parallel computation for pathlines and isosurfaces. For instance, Ozer *et al.* [OWS*12] use a clustering algorithm to group interacting features and perform feature tracking in time-varying 3D fluid flow simulations. Friederici *et al.* [FKA*19] propose a memory-distributed parallel algorithm to finely sample the percolation function, which is used to study statistical properties of turbulent flows. Binyahib *et al.* [BPNC19] work toward parallelizing particle advection for flow visualization. Manten *et al.* [MVO10] explore data extraction and preprocessing at the source in parallel and evaluate their techniques of flow visualization via parallel generation of pathlines and parallel extraction of isosurfaces. However, to the best of our knowledge, a few works have focused on scalable computation and visualization of time-independent and time-independent flow topology, for instance, the extraction of topological skeleton in a scalable manner. This avenue of research could be promising.

7.4. Machine Learning

Machine learning is rapidly transforming the landscape of scientific visualization. Berger *et al.* [BLL19] synthesize and analyze volume-rendered images using Generative Adversarial Network (GAN). Hong *et al.* [HLY19] combine GAN with Convolutional Neural Networks (CNN) to synthesize high-resolution and perceptually authentic images directly without an explicit traditional rendering pipeline. Tkachev *et al.* [TFE19] use feed-forward neural networks to detect and visualize interesting behaviors in spatiotemporal volumes, for adaptive time step selection and analysis of ensemble similarity. Han and Wang [HW20] generate temporal high-resolution time-varying volume sequences from low-resolution ones using adversarial learning. He *et al.* [HWG*20] use a deep-learning-based surrogate model to support parameter space exploration for ensemble simulations that are visualized in situ.

Integrating approaches from time-dependent flow visualization with machine learning to devise new techniques, in our opinion, is an extremely promising direction. For instance, can we use machine learning to increase the explainability of time-dependent flow topology? In particular, can *feature learning* be used to automatically discover topological features across time, therefore replacing classic feature detection and tracking algorithms?

7.5. Reproducibility

Flow topology is an area of scientific visualization where there are only few available open source softwares such as ParaView [FMT*11], VTK [SML06], and the topology toolkit [TFL*17]. In addition, reproducing the techniques among

the plethora of papers in the area is extremely hard – if even possible – without insider details. The lack of truly comprehensive toolkits that include robust, easy-to-use, generic implementations of existing methods is a key problem for their acceptance and adoption. The classical vector field topology was not added to the topology toolkit [TFL*17] until 2019, and VTK [SLM04, ABB*10] is still in the process of integrating it as of now. To accelerate the forward progress in flow topology, researchers should be encouraged, endorsed, and even rewarded for providing complete implementation of their techniques therefore allowing replication of their results.

8. Conclusion

In this paper, we aim to go beyond a simple classification or taxonomy of existing works, instead, we propose a mathematical framework that helps in explaining, describing, comparing, and discussing existing techniques. While existing surveys share some resemblance to our classification based on the approaches, our paper differs significantly from existing works in the sense that we methodically collect desirable mathematical properties to interpret physical meaningfulness for time-dependent flow visualization, and provably correlate such properties with selective research papers. To the best of our knowledge, this is the first time mathematical proofs are used to infer properties of flow visualization from characteristics of existing approaches, which subsequently help to interpret their physical meaningfulness.

After surveying the existing works on time-dependent flow topology and its mathematical properties, we see two main trends in filling the existing research gaps:

- As time passes and research advances, proposed methods in the visualization community tend to satisfy more and more of the desirable properties. This trend can be seen in the shift from red to green as we go down the tables.
- There is no current approach that satisfies all desirable properties. The two most promising approaches so far are reference frame adaption, which lacks Lagrangian invariance; and the categorization of pathlines, which does not coincide with the steady vector field topology.

For the future, we see great potential in studying the works from fluid dynamics and dynamical systems for inspirations on physically meaningful generalizations of time-dependent flow topology. Furthermore, we notice research gaps in combining time-dependent flow topology with uncertainty, scalability, and machine learning.

References

[ABB*10] AVILA L. S., BARRE S., BLUE R., GEVECI B., HENDERSON A., HOFFMAN W. A., KING B., LAW C. C., MARTIN K. M., SCHROEDER W. J.: *The VTK User's Guide*. Kitware New York, 2010. 21

[AE13] ATHAWALE T., ENTEZARI A.: Uncertainty quantification in linear interpolation for isosurface extraction. *IEEE Transactions on VIsualization and Computer Graphics 19*, 12 (2013), 2723–2732. 20

[AJ19] ATHAWALE T., JOHNSON C. R.: Probabilistic asymptotic decider for topological ambiguity resolution in level-set extraction for uncertain 2d data. *IEEE Transactions on Visualization and Computer Graphics 25*, 1 (2019), 1163–1172. 20

[AMJ*19] ATHAWALE T., MALJOVEC D., JOHNSON C. R., PASCUCCI V., WANG B.: Uncertainty visualization of 2d morse complex ensembles using statistical summary maps. *arXiv:1912.06341* (2019). 20

[ASE16] ATHAWALE T., SAKHAEE E., ENTEZARI A.: Isosurface visualization of data with nonparametric models for uncertainty. *IEEE Transactions on VIsualization and Computer Graphics 19*, 12 (2016), 2723–2732. 20

[BDBR*19] BUJACK R., DUTTA S., BAEZA ROJO I., ZHANG D., GÜNTHER T.: Objective Finite-Time Saddles and their Connection to FTLE. In *EuroVis 2019 - Short Papers* (2019), Johansson J., Sadlo F., Marai G. E., (Eds.), The Eurographics Association, pp. 49–53. 3, 4, 7, 9, 10, 13

[BDZG19] BUJACK R., DUTTA S., ZHANG D., GÜNTHER T.: Objective Finite-Time Flow Topology from Flowmap Expansion and Contraction. In *Topology-Based Methods in Visualization (TopoInVis 2019) Nyköping, Sweden* (2019). 3, 4, 7, 9, 10, 13, 16, 17

[BHJ16] BUJACK R., HLAWITSCHKA M., JOY K. I.: Topology-Inspired Galilean Invariant Vector Field Analysis. In *Proceedings of the IEEE Pacific Visualization Symposium, PacificVis 2016 in Taipei, Taiwan* (2016), pp. 72–79. 3, 4, 10, 11, 12, 17

[BJB*12] BHATIA H., JADHAV S., BREMER P., CHEN G., LEVINE J., NONATO L., PASCUCCI V.: Flow visualization with quantified spatial and temporal errors using edge maps. *IEEE Transactions on Visualization and Computer Graphics 18*, 9 (2012), 1383–1396. 20

[BK17] BANISCH R., KOLTAI P.: Understanding the geometry of transport: Diffusion maps for lagrangian trajectory data unravel coherent sets. *Chaos: An Interdisciplinary Journal of Nonlinear Science 27*, 3 (2017), 035804. 19

[BLL19] BERGER M., LI J., LEVINE J. A.: A generative model for volume rendering. *IEEE Transactions on Visualization and Computer Graphics 25*, 4 (2019), 1636–1650. 20

[BMC96] BLACKBURN H. M., MANSOUR N. N., CANTWELL B. J.: Topology of fine-scale motions in turbulent channel flow. *Journal of Fluid Mechanics 310* (1996), 269–292. 18

[BPB14] BHATIA H., PASCUCCI V., BREMER P.-T.: The natural helmholtz-hodge decomposition for open-boundary flow analysis. *IEEE transactions on visualization and computer graphics 20*, 11 (2014), 1566–1578. 3, 6, 7, 8, 14

[BPKB14] BHATIA H., PASCUCCI V., KIRBY R. M., BREMER P.-T.: Extracting features from time-dependent vector fields using internal reference frames. In *Computer graphics forum* (2014), vol. 33, Wiley Online Library, pp. 21–30. 3, 6, 7, 8, 14

[BPNC19] BINYAHIB R., PUGMIRE D., NORRIS B., CHILDS H.: A lifeline-based approach for work requesting and parallel particle advection. *IEEE 9th Symposium on Large Data Analysis and Visualization (LDAV)* (2019). 20

[BW09] BRANICKI M., WIGGINS S.: An adaptive method for computing invariant manifolds in non-autonomous, three-dimensional dynamical systems. *Physica D: Nonlinear Phenomena 238*, 16 (2009), 1625–1657. 18

[Can93] CANTWELL B. J.: On the behavior of velocity gradient tensor invariants in direct numerical simulations of turbulence. *Physics of Fluids A: Fluid Dynamics 5*, 8 (1993), 2008–2013. 18

[CC00] CHACIN J. M., CANTWELL B. J.: Dynamics of a low reynolds number turbulent boundary layer. *Journal of Fluid Mechanics 404* (2000), 87–115. 18

[CCK96] CHACÍN J. M., CANTWELL B. J., KLINE S. J.: Study of turbulent boundary layer structure using the invariants of the velocity gradient tensor. *Experimental thermal and fluid science 13*, 4 (1996), 308–317. 18

[CL93] CABRAL B., LEEDOM L. C.: Imaging vector fields using line integral convolution. In *Proceedings of the 20th annual conference on Computer graphics and interactive techniques* (1993), SIGGRAPH '93, ACM, pp. 263–270. doi:10.1145/166117.166151. 4, 7, 10

[CMLZ08] CHEN G., MISCHAIKOW K., LARAMEE R. S., ZHANG E.: Efficient morse decompositions of vector fields. *IEEE Transactions on Visualization and Computer Graphics (TVCG) 14*, 4 (2008), 848–862. 19

[CMS99] CARD S. K., MACKINLAY J. D., SHNEIDERMAN B.: *Readings in information visualization - using vision to think*. Academic Press, 1999. 18

[Cod12] CODDINGTON E. A.: *An introduction to ordinary differential equations*. Courier Corporation, 2012. 13

[CPC90] CHONG M. S., PERRY A. E., CANTWELL B. J.: A general classification of three-dimensional flow fields. *Physics of Fluids A: Fluid Dynamics 2*, 5 (1990), 765–777. 18

[CSP*98] CHONG M. S., SORIA J., PERRY A., CHACIN J., CANTWELL B., NA Y.: Turbulence structures of wall-bounded shear flows found using dns data. *Journal of Fluid Mechanics 357* (1998), 225–247. 18

[CWS*19] CARR H. A., WEBER G. H., SEWELL C. M., RÜBE O., FASEL P., AHRENS J. P.: Scalable contour tree computation by data parallel peak pruning. *IEEE Transactions on Visualization and Computer Graphics* (2019). 20

[CWSA16] CARR H. A., WEBER G. H., SEWELL C. M., AHRENS J. P.: Parallel peak pruning for scalable smp contour tree computation. *IEEE 6th Symposium on Large Data Analysis and Visualization (LDAV)* (2016). 20

[DJJ14] DAVID G., JOSEPH S., JULIEN T.: Mandatory critical points of 2D uncertain scalar fields. *Computer Graphics Forum 33*, 3 (2014), 31–40. 20

[FD03] FROYLAND G., DELLNITZ M.: Detecting and locating near-optimal almost-invariant sets and cycles. *SIAM J. Sci. Comput.* (2003), 1839. 19

[FFST19] FAVELIER G., FARAJ N., SUMMA B., TIERNY J.: Persistence atlas for critical point variability in ensembles. *IEEE Transactions on Visualization and Computer Graphics 25*, 1 (2019), 1152–1162. 20

[FH12] FARAZMAND M., HALLER G.: Computing lagrangian coherent structures from their variational theory. *Chaos: An Interdisciplinary Journal of Nonlinear Science 22*, 1 (2012), 013128. 19

[FH13] FARAZMAND M., HALLER G.: Attracting and repelling lagrangian coherent structures from a single computation. *Chaos: An Interdisciplinary Journal of Nonlinear Science 23*, 2 (2013), 023101. 19

[FKA*19] FRIEDERICI A., KÖPP W., ATZORI M., VINUESA R., SCHLATTER P., WEINKAUF T.: Distributed percolation analysis for turbulent flows. *IEEE 9th Symposium on Large Data Analysis and Visualization (LDAV)* (2019). 20

[FKS*10] FUCHS R., KEMMLER J., SCHINDLER B., WASER J., SADLO F., HAUSER H., PEIKERT R.: Toward a Lagrangian vector field topology. In *Computer Graphics Forum* (2010), vol. 29, Wiley Online Library, pp. 1163–1172. 3, 4, 10, 11, 12, 16

[FMT*11] FABIAN N., MORELAND K., THOMPSON D., BAUER A. C., MARION P., GEVECIK B., RASQUIN M., JANSEN K. E.: The ParaView coprocessing library: A scalable, general purpose in situ visualization library. *IEEE Symposium on Large Data Analysis and Visualization* (2011). 20

[FPG14] FROYLAND G., PADBERG-GEHLE K.: Almost-invariant and finite-time coherent sets: directionality, duration, and diffusion. In *Ergodic Theory, Open Dynamics, and Coherent Structures*. Springer, 2014, pp. 171–216. 19

[Fro01] FROYLAND G.: Extracting dynamical behavior via markov models. In *Nonlinear Dynamics and Statstics: Proceedings, Newton Institute, Cambridge 1998*, Mees A., (Ed.). Birkhäuser, Boston, MA, 2001, pp. 281–321. 19

[Fro12] FROYLAND G.: An analytic framework for identifying finite-time coherent sets in time-dependent dynamical systems. arXiv:1210.7418v1, 2012. 19

[Fro13] FROYLAND G.: An analytic framework for identifying finite-time coherent sets in time-dependent dynamical systems. *Physica D: Nonlinear Phenomena 250* (2013), 1–19. 19

[FSM10] FROYLAND G., SANTITISSADEKRN N., MONAHAN A.: Transport in time-dependent dynamical systems: Finite-time coherent sets. *Chaos 20* (2010), 043116. 19

[GGT17] GÜNTHER T., GROSS M., THEISEL H.: Generic objective vortices for flow visualization. *ACM Transactions on Graphics (TOG) 36*, 4 (2017), 141. 3, 4, 6, 7, 8

[GT18] GÜNTHER T., THEISEL H.: The state of the art in vortex extraction. In *Computer Graphics Forum* (2018), vol. 37, Wiley Online Library, pp. 149–173. 2

[GTS04] GARTH C., TRICOCHE X., SCHEUERMANN G.: Tracking of vector field singularities in unstructured 3d time-dependent datasets. In *Visualization, 2004. IEEE* (2004), IEEE, pp. 329–336. 2, 6, 7, 11

[Hal00] HALLER G.: Finding finite-time invariant manifolds in two-dimensional velocity fields. *Chaos: An Interdisciplinary Journal of Nonlinear Science 10*, 1 (2000), 99–108. 8, 19

[Hal02a] HALLER G.: Lagrangian Coherent Structures from Approximate Velocity Data. *Physics of Fluids 14* (2002), 1851–1861. 8

[Hal02b] HALLER G.: Lagrangian coherent structures from approximate velocity data. *Physics of fluids 14*, 6 (2002), 1851–1861. 13

[Hal05] HALLER G.: An objective definition of a vortex. *Journal of Fluid Mechanics 525* (2005), 1–26. 4

[Hal15] HALLER G.: Lagrangian coherent structures. *Annual Review of Fluid Mechanics 47* (2015), 137–162. 3, 10, 17, 19

[HBV13] HALLER G., BERON-VERA F. J.: Coherent lagrangian vortices: The black holes of turbulence. *Journal of Fluid Mechanics 731* (2013). 19

[HCJ*14] HANSEN C. D., CHEN M., JOHNSON C. R., KAUFMAN A. E., HAGEN H. (Eds.): *Scientific Visualization: Uncertainty, Multifield, Biomedical, and Scalable Visualization*. Springer-Verlag London, 2014. 20

[HFB*17] HADJIGHASEM A., FARAZMAND M., BLAZEVSKI D., FROYLAND G., HALLER G.: A critical comparison of lagrangian methods for coherent structure detection. *Chaos: An Interdisciplinary Journal of Nonlinear Science 27*, 5 (2017), 053104. 2, 3, 4, 13, 19

[HH89] HELMAN J., HESSELINK L.: Representation and display of vector field topology in fluid flow data sets. *Computer 22*, 8 (1989), 27–36. 1, 2, 4, 6, 7, 11, 12

[HH90] HELMAN J. L., HESSELINK L.: Surface representations of two- and three-dimensional fluid flow topology. In *Proceedings of the 1st conference on Visualization'90* (1990), IEEE Computer Society Press, pp. 6–13. 2, 6, 7, 11

[HHC*13] HUETTENBERGER L., HEINE C., CARR H., SCHEUERMANN G., GARTH C.: Towards multifield scalar topology based on pareto optimality. *Computer Graphics Forum 32*, 3 (2013), 341–350. 20

[HKTH16] HADJIGHASEM A., KARRASCH D., TERAMOTO H., HALLER G.: Spectral-clustering approach to lagrangian vortex detection. *Physical Review E 93*, 6 (2016), 063107. 3, 19

[HLH*16a] HEINE C., LEITTE H., HLAWITSCHKA M., IURICICH F., DE FLORIANI L., SCHEUERMANN G., HAGEN H., GARTH C.: A survey of topology-based methods in visualization. *Computer Graphics Forum 35*, 3 (2016), 643–667. 2, 3

[HLH*16b] HEINE C., LEITTE H., HLAWITSCHKA M., IURICICH F., DE FLORIANI L., SCHEUERMANN G., HAGEN H., GARTH C.: A survey of topology-based methods in visualization. *Computer Graphics Forum 35*, 3 (2016), 643–667. 20

[HLY19] HONG F., LIU C., YUAN X.: DNN-VolVis: Interactive volume visualization supported by deep neural network. *IEEE Pacific Visualization Symposium* (2019). 20

[HMTR18] HADWIGER M., MLEJNEK M., THEUSSL T., RAUTEK P.: Time-dependent flow seen through approximate observer killing fields. *IEEE transactions on visualization and computer graphics 25*, 1 (2018), 1257–1266. 3, 4, 7, 8, 14, 15

[HRHB17] HEIL M., ROSSO J., HAZEL A. L., BRØNS M.: Topological fluid mechanics of the formation of the kármán-vortex street. *Journal of Fluid Mechanics 812* (2017), 199–221. 19

[HW20] HAN J., WANG C.: TSR-TVD: Temporal super-resolution for time-varying data analysis and visualization. *IEEE Transactions on Visualization and Computer Graphics 26*, 1 (2020), 205–215. 20

[HWG*20] HE W., WANG J., GUO H., WANG K.-C., SHEN H.-W., RAJ M., NASHED Y. S. G., PETERKA T.: InSituNet: Deep image synthesis for parameter space exploration of ensemble simulations. *IEEE Transactions on Visualization and Computer Graphics 26*, 1 (2020), 23 – 33. 20

[HY00] HALLER G., YUAN G.: Lagrangian coherent structures and mixing in two-dimensional turbulence. *Phys. D 147*, 3-4 (Dec. 2000), 352–370. URL: http://dx.doi.org/10.1016/S0167-2789(00)00142-1, doi:10.1016/S0167-2789(00)00142-1. 19

[ISW02] IDE K., SMALL D., WIGGINS S.: Distinguished hyperbolic trajectories in time-dependent fluid flows: analytical and computational approach for velocity fields defined as data sets. *Nonlinear Processes in Geophysics 9*, 3/4 (2002), 237–263. 18

[KHNH11] KASTEN J., HOTZ I., NOACK B. R., HEGE H.-C.: On the extraction of long-living features in unsteady fluid flows. In *Topological Methods in Data Analysis and Visualization*, Pascucci V., Tricoche X., Hagen H., Tierny J., (Eds.), Mathematics and Visualization. Springer Berlin Heidelberg, 2011, pp. 115–126. URL: http://dx.doi.org/10.1007/978-3-642-15014-2_10, doi:10.1007/978-3-642-15014-2_10. 3, 4, 9, 12, 16

[KPH*09] KASTEN J., PETZ C., HOTZ I., NOACK B. R., HEGE H.-C.: Localized finite-time lyapunov exponent for unsteady flow analysis. In *VMV* (2009), pp. 265–276. 11

[Kra10] KRAUS M.: Visualization of uncertain contour trees. *Proceedings of the International Conference on Information Visualization Theory and Applications* (2010), 132–139. 20

[KRH*16] KASTEN J., REININGHAUS J., HOTZ I., HEGE H.-C., NOACK B. R., DAVILLER G., MORZYNSKI M.: Acceleration feature points of unsteady shear flows. *Archives of Mechanics 68* (2016), 55–80. 3, 9, 10, 12

[LCJK*09] LARAMEE R. S., CHEN G., JANKUN-KELLY M., ZHANG E., THOMPSON D.: Bringing topology-based flow visualization to the application domain. *Topology-Based Methods in Visualization II Mathematics and Visualization* (2009). 2

[LHZP07] LARAMEE R. S., HAUSER H., ZHAO L., POST F. H.: Topology-based flow visualization, the state of the art. In *Topology-based Methods in Visualization* (2007), Hauser H., Hagen H., Theisel H., (Eds.), pp. 1–19. 2

[Liu02] LIU I.: *Continuum Mechanics*. Advanced Texts in Physics. Springer, 2002. URL: https://books.google.com/books?id=-gWqM4uMV6wC. 11

[Liu03] LIU I.-S.: On the transformation property of the deformation gradient under a change of frame. *Journal of elasticity 71*, 1-3 (2003), 73–80. 13

[Lug79] LUGT H. J.: The dilemma of defining a vortex. In *Recent developments in theoretical and experimental fluid mechanics*. Springer, 1979, pp. 309–321. 1, 7

[MB14] MA T., BOLT E. M.: Differential geometry perspective of shape coherence and curvature evolution by finite-time nonhyperbolic splitting. *Siam J. Applied Dynamical Systems 13*, 3 (2014), 1106–1136. 19

[MBES16] MACHADO G., BOBLEST S., ERTL T., SADLO F.: Space-time bifurcation lines for extraction of 2d lagrangian coherent structures. In *Computer Graphics Forum* (2016), vol. 35, Wiley Online Library, pp. 91–100. 3, 4, 7, 11, 12, 17

[Mis02] MISCHAIKOW K.: Topological techniques for efficient rigorous computations in dynamics. In *Acta Numerica*. Cambridge University Press, 2002, pp. 435–477. URL: citeseer.ist.psu.edu/mischaikow01topological.html, doi:10.1017/S0962492902000065. 19

[MSE13] MACHADO G. M., SADLO F., ERTL T.: Local extraction of bifurcation lines. In *VMV* (2013), Citeseer, pp. 17–24. 11

[MVO10] MANTEN S., VETTER M., OLBRICH S.: Evaluation of a scalable in-situ visualization system approach in a parallelized computational fluid dynamics application. In *Virtual Realities: Dagstuhl Seminar 2008*, Coquillart S., Brunnett G., Welch G., (Eds.). Springer Science & Business Media, 2010. 20

[MW99] MEZIĆ I., WIGGINS S.: A method for visualization of invariant sets of dynamical systems based on the ergodic partition. *Chaos: An Interdisciplinary Journal of Nonlinear Science 9*, 1 (1999), 213–218. 13

[MW13] MOROZOV D., WEBER G.: Distributed merge trees. *Proceedings Annual Symposium on Principles and Practice of Parallel Programming,*, 93-102 (2013). 20

[MW14] MIHAI M., WESTERMANN R.: Visualizing the stability of critical points in uncertain scalar fields. *Computers and Graphics 41* (2014), 13 – 25. doi:https://doi.org/10.1016/j.cag.2014.01.007. 20

[MWCM13] MANCHO A. M., WIGGINS S., CURBELO J., MENDOZA C.: Lagrangian descriptors: A method for revealing phase space structures of general time dependent dynamical systems. *Communications in Nonlinear Science and Numerical Simulation 18*, 12 (2013), 3530–3557. 19

[NNN11] NAGARAJ S., NATARAJAN V., NANJUNDIAH R. S.: A gradient-based comparison measure for visual analysis of multi-field data reconstruction of gradient in volume rendering. *Eurographics/IEEE Symposium on Visualization 30*, 3 (2011). 20

[OGHT10] OTTO M., GERMER T., HEGE H.-C., THEISEL H.: Uncertain 2D vector field topology. *Computer Graphics Forum 29*, 2 (2010), 347–356. 20

[OGT11] OTTO M., GERMER T., THEISEL H.: Uncertain topology of 3D vector fields. In *IEEE Pacific Visualization Symposium* (2011), pp. 67–74. 20

[OWS*12] OZER S., WEI J., SILVER D., MA K.-L., MARTIN P.: Group dynamics in scientific visualization. *IEEE Symposium on Large Data Analysis and Visualization (LDAV)* (2012). 20

[PC94a] PERRY A., CHONG M.: Topology of flow patterns in vortex motions and turbulence. *Applied Scientific Research 53*, 3 (1994), 357–374. 1, 3, 4, 7

[PC94b] PERRY A., CHONG M.: Topology of flow patterns in vortex motions and turbulence. *Applied Scientific Research 53*, 3 (1994), 357–374. 4

[PH13] PÖTHKOW K., HEGE H.-C.: Nonparametric models for uncertainty visualization. *Computer Graphics Forum 32*, 3.2 (2013), 131–140. 20

[PMW13] PFAFFELMOSER T., MIHAI M., WESTERMANN R.: Visualizing the variability of gradients in uncertain 2D scalar fields. *IEEE Transactions on Visualization and Computer Graphics 19*, 11 (2013), 1948–1961. 20

[PPF*11a] POBITZER A., PEIKERT R., FUCHS R., SCHINDLER B., KUHN A., THEISEL H., MATKOVIC K., HAUSER H.: The state of the art in topology-based visualization of unsteady flow. *Computer Graphics Forum 30*, 6 (2011), 1789–1811. 2, 3

[PPF*11b] POBITZER A., PEIKERT R., FUCHS R., SCHINDLER B., KUHN A., THEISEL H., MATKOVIĆ K., HAUSER H.: The state of the art in topology-based visualization of unsteady flow. In *Computer Graphics Forum* (2011), vol. 30, Wiley Online Library, pp. 1789–1811. 3, 4

[PVH*03] POST F. H., VROLIJK B., HAUSER H., LARAMEE R. S., DOLEISCH H.: The state of the art in flow visualisation: Feature extraction and tracking. In *Computer Graphics Forum* (2003), vol. 22, Wiley Online Library, pp. 775–792. 2

[PWH11] PÖTHKOW K., WEBER B., HEGE H.-C.: Probabilistic marching cubes. *Computer Graphics Forum 30*, 3 (2011), 931–940. 20

[RG20] ROJO I. B., GÜNTHER T.: Vector field topology of time-dependent flows in a steady reference frame. *IEEE Transactions on Visualization and Computer Graphics 26*, 1 (2020). doi:10.1109/TVCG.2019.2934375. 3, 4, 7, 8, 15

[RH11] REININGHAUS J., HOTZ I.: Combinatorial 2d vector field topology extraction and simplification. *Topological Methods in Data Analysis and Visualization* (2011), 103–114. 16

[RKWH12] REININGHAUS J., KASTEN J., WEINKAUF T., HOTZ I.: Efficient computation of combinatorial feature flow fields. *IEEE Transactions on Visualization and Computer Graphics 18*, 9 (2012), 1563–1573. 2, 3, 6, 7, 10, 11, 12

[Rot00] ROTH M.: *Automatic extraction of vortex core lines and other line type features for scientific visualization*, vol. 2. Hartung-Gorre, 2000. 11

[RP98] ROTH M., PEIKERT R.: A higher-order method for finding vortex core lines. In *Proceedings of the conference on Visualization'98* (1998), IEEE Computer Society Press, pp. 143–150. 11

[RSM16] RAMON S. MARTINS ANSELMO SOEIRO PEREIRA G. M. L. T. R. L. T.: An objective perspective for classic flow classification criteria. *Elsevier Masson SAS* (2016). doi:http://dx.doi.org/10.1016/j.crme.2015.08.002. 4

[RSPB11] RYPINA I. I., SCOTT S., PRATT L. J., BROWN M. G.: Investigating the connection between complexity of isolated trajectories and lagrangian coherent structures. *Nonlinear Processes in Geophysics 18*, 6 (2011), 977–987. 19

[SH95] SUJUDI D., HAIMES R.: Identification of swirling flow in 3-D vector fields. In *12th Computational Fluid Dynamics Conference*. American Institute of Aeronautics and Astronautics, 1995. doi:10.2514/6.1995-1715. 4

[Shn03] SHNEIDERMAN B.: The eyes have it: A task by data type taxonomy for information visualizations. In *The Craft of Information Visualization*. Elsevier, 2003, pp. 364–371. 5

[SJ06] SERWAY R., JEWETT J.: *Principles of Physics: A Calculus-Based Text*. No. Bd. 1 in Available 2010 Titles Enhanced Web Assign Series. Cengage Learning, 2006. URL: https://books.google.com/books?id=1DZz341Pp50C. 11

[SLM04] SCHROEDER W. J., LORENSEN B., MARTIN K.: *The visualization toolkit: an object-oriented approach to 3D graphics*. Kitware, 2004. 21

[SLM05] SHADDEN S. C., LEKIEN F., MARSDEN J. E.: Definition and properties of lagrangian coherent structures from finite-time lyapunov exponents in two-dimensional aperiodic flows. *Physica D: Nonlinear Phenomena 212*, 3 (2005), 271–304. 3, 19

[SM17] SMIRNOV D., MOROZOV D.: Triplet merge trees. In *Mathematics and Visualization*. Springer, 2017. 20

[SML06] SCHROEDER W., MARTIN K., LORENSEN B.: *The Visualization Toolkit*, 4th ed. Kitware, 2006. 20

[SMN12] SHIVASHANKAR N., M S., NATARAJAN V.: Parallel computation of 2d Morse-Smale complexes. *IEEE Transactions on Visualization and Computer Graphics 18*, 10 (2012), 1757–1770. 20

[SN12] SHIVASHANKAR N., NATARAJAN V.: Parallel computation of 3d morse-smale complexes. *Computer Graphic Forum 31*, 3pt1 (2012), 965–974. 20

[Son13] SONG Y.: A note on galilean invariants in semi-relativistic electromagnetism. *arXiv preprint arXiv:1304.6804* (2013). 11

[SSC*94] SORIA J., SONDERGAARD R., CANTWELL B., CHONG M., PERRY A.: A study of the fine-scale motions of incompressible time-developing mixing layers. *Physics of Fluids 6*, 2 (1994), 871–884. 18

[SW10] SADLO F., WEISKOPF D.: Time-dependent 2-d vector field topology: An approach inspired by lagrangian coherent structures. In *Computer Graphics Forum* (2010), vol. 29, Wiley Online Library, pp. 88–100. 3, 4, 7, 8, 9, 10, 11, 13, 16

[SW14] SKRABA P., WANG B.: Interpreting feature tracking through the lens of robustness. In *Topological Methods in Data Analysis and Visualization III: Theory, Algorithms, and Applications (Proceedings of TopoInVis 2013)*, Bremer P.-T., Hotz I., Pascucci V., Peikert R., (Eds.). Springer, 2014, pp. 19–38. 2, 6, 7, 11

[SWTH07] SAHNER J., WEINKAUF T., TEUBER N., HEGE H.-C.: Vortex and strain skeletons in eulerian and lagrangian frames. *IEEE Transactions on Visualization and Computer Graphics 13*, 5 (2007). 4

[TFE19] TKACHEV G., FREY S., ERTL T.: Local prediction models for spatiotemporal volume visualization. *IEEE Transactions on Visualization and Computer Graphics* (2019). 20

[TFL*17] TIERNY J., FAVELIER G., LEVINE J. A., GUEUNET C., MICHAUX M.: The topology toolkit. *IEEE Transactions on Visualization and Computer Graphics 24*, 1 (2017), 832–842. 20, 21

[TLB*11] THOMPSON D., LEVINE J. A., BENNETT J. C., BREMER P.-T., GYULASSY A., PASCUCCI V.: Analysis of large-scale scalar data using hixels. *IEEE Symposium on Large Data Analysis and Visualization* (2011). 20

[TN04] TRUESDELL C., NOLL W.: The non-linear field theories of mechanics. In *The non-linear field theories of mechanics*. Springer, 2004, pp. 1–579. 4, 8, 11

[TS03] THEISEL H., SEIDEL H.-P.: Feature flow fields. In *VisSym* (2003), vol. 3, pp. 141–148. 2, 6, 7, 11

[TSH01] TRICOCHE X., SCHEUERMANN G., HAGEN H.: Topology-based visualization of time-dependent 2d vector fields. In *VisSym* (2001), pp. 117–126. 2, 6, 7, 11

[TWHS04] THEISEL H., WEINKAUF T., HEGE H.-C., SEIDEL H.-P.: Stream line and path line oriented topology for 2d time-dependent vector fields. In *Proceedings of the conference on Visualization'04* (2004), IEEE Computer Society, pp. 321–328. 2, 3, 6, 7, 10, 11, 15, 16

[TWHS05] THEISEL H., WEINKAUF T., HEGE H.-C., SEIDEL H.-P.: Topological methods for 2D time-dependent vector fields based on stream lines and path lines. *Visualization and Computer Graphics, IEEE Transactions on 11*, 4 (July 2005), 383–394. doi:10.1109/TVCG.2005.68. 2, 3, 6, 7, 9, 10, 11, 15, 16

[TWSH02] TRICOCHE X., WISCHGOLL T., SCHEUERMANN G., HAGEN H.: Topology tracking for the visualization of time-dependent two-dimensional flows. *Computers & Graphics 26*, 2 (2002), 249–257. 2, 6, 7, 11

[USE12] UFFINGER M., SADLO F., ERTL T.: A time-dependent vector field topology based on streak surfaces. *IEEE Transactions on Visualization and Computer Graphics 19*, 3 (2012), 379–392. 3, 4, 7, 9, 10, 13, 16

[WBPRH17] WANG B., BUJACK R., PAUL ROSEN PRIMOZ SKRABA H. B., HAGEN H.: Interpreting galilean invariant vector field analysis via extended robustness. In *Topology-Based Methods in Visualization (TopoInVis 2017) Tokyo, Japan* (2017). 3, 4, 11, 12, 18

[WCW*11] WIEBEL A., CHAN R., WOLF C., ROBITZKI A., STEVENS A., SCHEUERMANN G.: Topological flow structures in a mathematical model for rotation-mediated cell aggregation. In *Topological Methods in Data Analysis and Visualization*. Springer, 2011, pp. 193–204. 3, 8, 9, 10, 13, 16

[WGS02] WIEBEL A., GARTH C., SCHEUERMANN G.: Computation of localized flow for steady and unsteady vector fields and its applications.

IEEE Trans. Visualization and Computer Graphics 1, 8 (2002). 3, 6, 7, 8, 14

[Wie08] WIEBEL A.: Localized flow, particle tracing, and topological separation analysis for flow visualization. In *PhD dissertation* (2008). 4

[WMK13] WHITAKER R., MIRZARGAR M., KIRBY R.: Contour box-plots: A method for characterizing uncertainty in feature sets from simulation ensembles. *IEEE Transactions on Visualization and Computer Graphics 19*, 12 (2013), 2713–2722. 20

[WRS*13] WANG B., ROSEN P., SKRABA P., BHATIA H., PASCUCCI V.: Visualizing robustness of critical points for 2d time-varying vector fields. In *Computer Graphics Forum* (2013), vol. 32, Wiley Online Library, pp. 221–230. 11

[WRT18] WILDE T., RÖSSI C., THEISEL H.: Recirculation surfaces for flow visualization. *IEEE transactions on visualization and computer graphics 25*, 1 (2018), 946–955. 3, 9, 10, 13

[WS01] WISCHGOLL T., SCHEUERMANN G.: Detection and visualization of closed streamlines in planar flows. *IEEE Transactions on Visualization and Computer Graphics 7*, 2 (2001), 165–172. 6

[WSH01] WISCHGOLL T., SCHEUERMANN G., HAGEN H.: Tracking closed streamlines in time dependent planar flows. In *VMV* (2001), pp. 447–454. 2, 6, 7, 11

[WTS*07] WIEBEL A., TRICOCHE X., SCHNEIDER D., JAENICKE H., SCHEUERMANN G.: Generalized streak lines: Analysis and visualization of boundary induced vortices. *IEEE Transactions on Visualization and Computer Graphics 13*, 6 (2007), 1735–1742. 8

[WTVGP11] WEINKAUF T., THEISEL H., VAN GELDER A., PANG A.: Stable Feature Flow Fields. *IEEE Transactions on Visualization and Computer Graphics 17*, 6 (June 2011), 770–780. 2, 6, 7, 11

[WWL16] WANG W., WANG W., LI S.: From numerics to combinatorics: a survey of topological methods for vector field visualization. *Journal of Visualization 19*, 4 (2016), 727–752. 2

[WZ12] WU K., ZHANG S.: A contour tree based visualization for exploring data with uncertainty. *International Journal for Uncertainty Quantification 3*, 3 (2012), 203–223. 20

[YWM*20] YAN L., WANG Y., MUNCH E., GASPAROVIC E., WANG B.: A structural average of labeled merge trees for uncertainty visualization. *IEEE Transactions on Visualization and Computer Graphics 26*, 1 (2020), 832 – 842. 20

[ZAM15] ZHANG W., AGARWAL P. K., MUKHERJEE S.: Contour trees of uncertain terrains. *Proceedings of the 23rd SIGSPATIAL International Conference on Advances in Geographic Information Systems 43* (2015). 20

Short Biographies

Roxana Bujack is a staff scientist in the Data Science at Scale Team at Los Alamos National Laboratory. She graduated in mathematics and computer science and received her PhD in the Image and Signal Processing group at Leipzig University in Germany. Then, she worked as a postdoctoral researcher at IDAV at the University of California, Davis and at the Computer Graphics and HCI Group at the Technical University Kaiserslautern. Her research interests include visualization, pattern detection, flow fields, and color theory.

Lin Yan is a PhD student in Scientific Computing and Imaging (SCI) Institute, University of Utah. Her research interests in topological data analysis and visualization, and most of her work are under the guidance of Dr. Bei Wang Phillips.

Ingrid Hotz is currently a Professor in Scientific Visualization at the Linköping University in Sweden. She received her Ph.D. degree from the Computer Science Department at the University of Kaiserslautern, Germany. She worked as a postdoctoral researcher at IDAV at the University of California, Davis. Previous positions include leading a junior research group in visualization at the Zuse Institute Berlin and leading the scientific visualization group at the German Aerospace Center (DLR). Her research interests lie in data analysis and scientific visualization, ranging from basic research questions to effective solutions to visualization problems in applications. This includes developing and applying concepts originating from different areas of computer sciences and mathematics, such as computer graphics, computer vision, dynamical systems, computational geometry, and combinatorial topology.

Christoph Garth received his Ph.D. degree in computer science from Technische Universität Kaiserslautern in 2007. After four years as a postdoctoral researcher at the University of California, Davis, he rejoined TU Kaiserslautern and is now a full professor of Computer Science there. His research interests include large-scale data analysis and visualization, in situ visualization, topology-based visualization methods, and interdisciplinary applications of visualization.

Bei Wang is an assistant professor at the School of Computing and a faculty member at the Scientific Computing and Imaging (SCI) Institute, University of Utah. She received her Ph.D. in Computer Science from Duke University. She is interested in the analysis and visualization of large and complex data. Her research interests include topological data analysis, data visualization, computational topology, computational geometry, machine learning and data mining.